Chemical Geology 557 (2020) 119859

Contents lists available at ScienceDirect

Chemical Geology

journal homepage: www.elsevier.com/locate/chemgeo

Boron isotopic investigation of the Bayan Obo carbonatite complex: Insights into the source of mantle carbon and hydrothermal alteration

Corinne Kuebler[a,*], Antonio Simonetti[a], Wei Chen[b], Stefanie S. Simonetti[a]

[a] Department of Civil and Environmental Engineering and Earth Sciences, University of Notre Dame, Notre Dame, Indiana 46556, USA
[b] State Key Laboratory of Geological Processes and Mineral Resources, Faculty of Earth Science, China University of Geosciences, Wuhan 430074, China

ARTICLE INFO

Editor: Catherine Chauvel

Keywords:
Boron isotopes
Bayan Obo carbonatite complex
Magmatic origin
Enriched upper mantle source regions in Central China
Late-stage hydrothermal REE mineralization

ABSTRACT

Earth's largest rare earth element (REE) ore deposit at Bayan Obo, China, is hosted in a dolomitic marble of Mesoproterozoic age, the genesis of which remains controversial, whether it is of sedimentary or igneous origin. Evidence of Caledonian-age recrystallization further complicates the interpretation of geochemical data from this complex. This study provides new insights into the petrogenetic history of the Bayan Obo host dolomite by documenting major and trace element abundances, and the first-reported $\delta^{11}B$ values combined with radiogenic (Sr, Nd, Pb) and stable (C, O) isotope results. Boron abundances of the carbonates investigated are typical for carbonatites worldwide (0.4–1.1 ppm) and overlap with those for fresh (unaltered) mid-ocean ridge basalts (MORBs). Boron isotope ratios do not exhibit any systematic correlations with their corresponding B contents, light rare earth element (LREE) concentrations, $\delta^{13}C_{PDB}$ or $\delta^{18}O_{SMOW}$ compositions. For seven dolomite samples characterized by pristine $^{87}Sr/^{86}Sr_{(i)}$ values (< 0.70340), the $\delta^{11}B$ compositions range from −3.6 to −9.0‰, which vary between those for typical asthenospheric (MORB) mantle (−7.1 ± 0.9‰) and an enriched mantle source. The $\delta^{11}B$ values for the remaining samples span a wide range (−14.5 to −1.0‰) and given their corresponding more radiogenic $^{87}Sr/^{86}Sr_{(i)}$ compositions (> 0.70340) suggest hydrothermal alteration. Additionally, εNd_{CHUR} values (1.3 Ga) define two groups corresponding to pristine samples (−1.5 to 1.2) and those containing recrystallized REE-bearing phases (−3.0 to −12.6). Together, the major and trace element abundances, $\delta^{11}B$ values, and radiogenic isotope data for the host dolomitic marble at Bayan Obo are consistent with an upper mantle origin, and are best explained through the involvement and mixing of at least three distinct mantle reservoirs. When combined with radiogenic and B isotope results from other carbonatite complexes within China (Maoniuping, HYC- Huayangchuan, QMC- Qiganbulake mafic–ultramafic-carbonatite complex, Miaoya, TNCC- Trans-North China Carbonatites) of varying emplacement ages (between ~26 and ~2000 Ma), these all suggest derivation from enriched upper mantle source regions during the past ~2 billion years. Comparison of the initial Pb isotope ratios reported here for Bayan Obo carbonates to those from the 440 Ma Miaoya carbonatite complex may be attributed to either a significant increase in the upper mantle's $^{238}U/^{204}Pb$ ratio under present-day China over a ~900-million-year interval, or simply reflects derivation from distinct upper mantle sources.

1. Introduction

Carbonatites are alkali and carbon-rich igneous rocks of great economic interest due to their enrichment in strategic metals and elements, such as Sr, Nd, P, Ta, Nb, and rare Earth elements (REEs; e.g., Bell and Simonetti, 2010; Jones et al., 2013). These rocks are most often associated with intra-plate continental rift areas, but do occur in a number of different tectonic settings including oceanic environments and orogenic belts (Woolley, 1989; Woolley and Kjarsgaard, 2008). The origin of carbonatite melt is still subject to debate with three main mechanisms proposed: 1. Direct partial melting of a metasomatized upper mantle source (e.g., Gittins and Harmer, 2003; Bell and Simonetti, 2010), 2. As a product of liquid immiscibility from carbonated silicate melts (e.g., Lee and Wyllie, 1998; Lee et al., 2000), or 3. Generated by extreme melt differentiation from a parental carbonated silicate magma via fractional crystallization (e.g., Veksler et al., 1998; Mitchell, 2005; Cooper et al., 2011). The exact mantle source invoked by the first hypothesis is also contentious since two main competing interpretations exist; one advocates for carbonatite melt derivation from the subcontinental lithospheric mantle (SCLM; e.g., Bailey, 1993),

* Corresponding author.
E-mail addresses: ckuebler@nd.edu (C. Kuebler), simonetti.3@nd.edu (A. Simonetti), wchen@cug.edu.cn (W. Chen), simonetti.4@nd.edu (S.S. Simonetti).

https://doi.org/10.1016/j.chemgeo.2020.119859
Received 29 April 2020; Received in revised form 7 August 2020; Accepted 28 August 2020
Available online 01 September 2020

while the other involves an asthenospheric origin (e.g., Bell and Simonetti, 2010). Evidence from various radiogenic isotope studies of younger carbonatites (< 200 Ma) suggest the involvement of several mantle components in the generation of carbonatite magmas, principally HIMU (high-μ; $^{238}U/^{204}Pb$) and EMI (Enriched Mantle I; Zindler and Hart, 1986; Bell and Simonetti, 1996; Bell and Tilton, 2001; Bell and Simonetti, 2010); the latter components were attributed to the mantle sources of oceanic island basalts (OIBs) and mantle plumes (Zindler and Hart, 1986). Also, the exact origin of mantle carbon (C) within carbonatites is unknown and may represent a mixture of sources, as it could be juvenile, recycled, or both (e.g., carbonate minerals/fluids; Bell and Simonetti, 2010; Hulett et al., 2016).

Carbonatites are found on all continents with ≥500 occurrences worldwide, and span a wide range in age (~3.0 billion years ago to present-day; Woolley and Kjarsgaard, 2008), which allows them to monitor the chemical evolution of the Earth's upper mantle over billions of years (e.g., Bell et al., 1982). Moreover, their alkali-rich nature affects both the chemical and physical properties of the upper mantle due to metasomatism of the continental lithosphere, impacting many subsurface processes, such as partial melting and the distribution of incompatible trace elements (Bell and Blenkinsop, 1987; Simonetti et al., 1998; Bell and Simonetti, 2010). Additionally, the predominance of carbonate in these rocks directly ties their petrogenesis to the Earth's deep carbon cycle and the origin of mantle C (Bell and Simonetti, 2010; Hulett et al., 2016). For example, Bizzaro et al. (2002) argued for the presence of a long-lived, secluded, enriched mantle source based on the Hf isotopic data for ~3-billion-year-old carbonatite (Tupertalik, Greenland). This supports the notion that carbonatites (and kimberlites) can tap deep mantle sources containing recycled crustal materials via upwelling plumes (e.g., Smith et al., 2018). Thus, carbonatite magmatism may provide important insights into both ancient and present-day mantle processes, including deep carbon recycling.

Regardless of their exact petrogenesis, carbonatites are key REE economic resources with the world's largest REE deposit being the Bayan Obo carbonatite complex located in northern China (Fig. 1; Le Bas et al., 1992; Yuan et al., 1992; Le Bas et al., 1997). The Bayan Obo ore body is hosted in a dolomitic marble with an unclear origin, even after ~90 years of study. The main point of contention involves determining the exact derivation of the Bayan Obo host dolomite, whether it is sedimentary (Meng, 1982; Tu et al., 1985; Wang et al., 1994) or igneous in origin (Le Bas et al., 1997; Yang and Le Bas, 2004; Yang et al., 2011; Fan et al., 2016; Ren et al., 2019; Yang et al., 2019; Chen et al., 2020). More recently, Smith et al. (2015) argued for a multi-stage evolution of the complex, which involved intrusion of an alkaline igneous system within the sedimentary Bayan Obo Group sequence during Mesoproterozoic rifting (1.3 Ga). This was followed by Caledonian-aged metasomatism during the subduction of the Mongolian plate under the North China Craton (~450 Ma). This multi-step petrogenetic model integrates the mineralogy, field observations, geochronology and geochemistry of previous studies, and acknowledges that the petrogenesis of the area is complicated by regional deformation, metamorphism, and metasomatism (Smith et al., 2015; Ren et al., 2019).

Over the last few decades, boron and its isotopes have become a viable and reliable, non-traditional stable isotope system for tracking geological processes, including those in magmatic systems due to advances in analytical techniques (e.g., Marschall and Foster, 2017 and references therein). Importantly, boron has been linked to deep mantle carbon via investigations of boron-bearing blue diamonds (Gaillou et al., 2012; Smith et al., 2018). Its incompatible nature leads to a distinct depletion in the asthenospheric (MORB) mantle (≤1 ppm; Chaussidon and Jambon, 1994; Marschall et al., 2017) and enrichment in the continental crust (up to ~40 ppm; Kasemann et al., 2000). The relatively high mass difference (~10%) between ^{10}B and ^{11}B causes large natural variation in $\delta^{11}B$ (~100‰) ranging from −7.1 ± 0.9‰ in asthenospheric mantle (Marschall et al., 2017) to +39.6 ± 0.04‰ in modern seawater (Foster et al., 2010). While the isotopic signature of boron has yet to be well-established for carbonatites, preliminary data has revealed a temporal trend that spans the past ~2.1 billion years of Earth history (Hulett et al., 2016). Boron isotopic signatures for older carbonatites (> 300 Ma) are characterized by asthenospheric mantle values (−7.1 ± 0.9‰; Marschall et al., 2017), while younger carbonatites (< 300 Ma) show increased variation and exhibit more positive values (−4 to +5‰). The latter feature has been interpreted as indicating an increased presence of recycled boron-enriched material within the mantle source that gives rise to carbonatite magmas with increasing geologic time (Hulett et al., 2016). Moreover, when combined with more traditional, radiogenic (Nd, Pb, Sr) and stable (C, O) isotope signatures, boron isotope compositions provide valuable information about the chemical nature and the possible presence of subducted (recycled) crustal materials within their mantle source region (e.g., Hulett et al., 2016; Çimen et al., 2018, 2019).

This study reports for the first-time boron isotopic compositions for the Bayan Obo host dolomitic marble to provide further insights into its petrogenesis. The results presented here once again demonstrate the robust nature of boron within mantle-derived carbonates in maintaining their inherited mantle isotopic signature despite undergoing secondary processes, such as mid-amphibolite grade metamorphism and/or hydrothermal activity (e.g., Çimen et al., 2019). Additionally, the chemical and isotopic data from this study are compared with those from the younger Miaoya carbonatite complex (~440 Ma old; Çimen et al., 2018), several relatively proximal carbonatites (Fig. 1 inset; Huayangchuan (HYC), Trans-North China Carbonatites (TNCC), Maoniuping), and the distal Qiganbulake mafic–ultramafic-carbonatite complex (QMC), in order to examine the temporal, chemical evolution of the upper mantle in this region of present-day China over a period of ~900 million years.

2. Geological background

The Bayan Obo ore deposit is located on the northern border of the North China Craton (NCC) in Inner Mongolia, Northern China and lies south of the Central Asian Orogenic Belt (Fig. 1). Basement rocks at Bayan Obo consist of Archean mylonitic granite-gneiss, and Paleoproterozoic syenite, granodiorite and granite-gneiss (Fan et al., 2016). The orebody is typically considered to be part of a Mesoproterozoic metasedimentary sequence, the Bayan Obo Group, which contains sandstone, limestone, and slate (Fig. 1). This group represents sediments deposited during a period of marginal rifting from ~1.8 Ga to ~1.2 Ga and correlated to the breakup of the NCC from the supercontinent Columbia (Zhao et al., 2003; Zhai, 2004). An additional result of this rifting was the formation of mafic (basaltic to basaltic-trachy-andesitic) dyke swarms and carbonatite dykes throughout the region (Yang et al., 2009). The nearly 100 carbonatite dykes identified in the area vary from 0.5–2.0 m wide and 10–200 m long (Le Bas et al., 1992; Tao et al., 1998; Yang et al., 2011; Fan et al., 2014). These carbonatites intrude both the basement rocks and the Bayan Obo Group producing fenites from metasomatized country rock (Fan et al., 2016 and references wherein).

Bayan Obo's REE-Nb-Fe bearing ore is hosted within the Bayan Obo Group by a dolomitic marble typically termed as H8, that is overlain by K-rich slate (H9) and folded into a synclinal core (Fan et al., 2016 and references therein). The REE deposit is characterized by three exposed orebodies, Main, East, and West that have differing REE concentrations and distribution (Smith et al., 2015; Fan et al., 2016). The H8 marble shows significant variations in both mineralogy and geochemistry. The major mineral constituents are dolomite and calcite with abundant apatite, monazite, barite, bastnaesite, and magnetite (Le Bas et al., 2007; Smith et al., 2015; Liu et al., 2018a). H8 can additionally be defined as fine-grained (FG), coarse-grained (CG), and heterogeneous (HG) marble based on grain size, and these are characterized by distinct chemical and isotopic signatures (Bai and Zhongxin, 1985; Le Bas et al.,

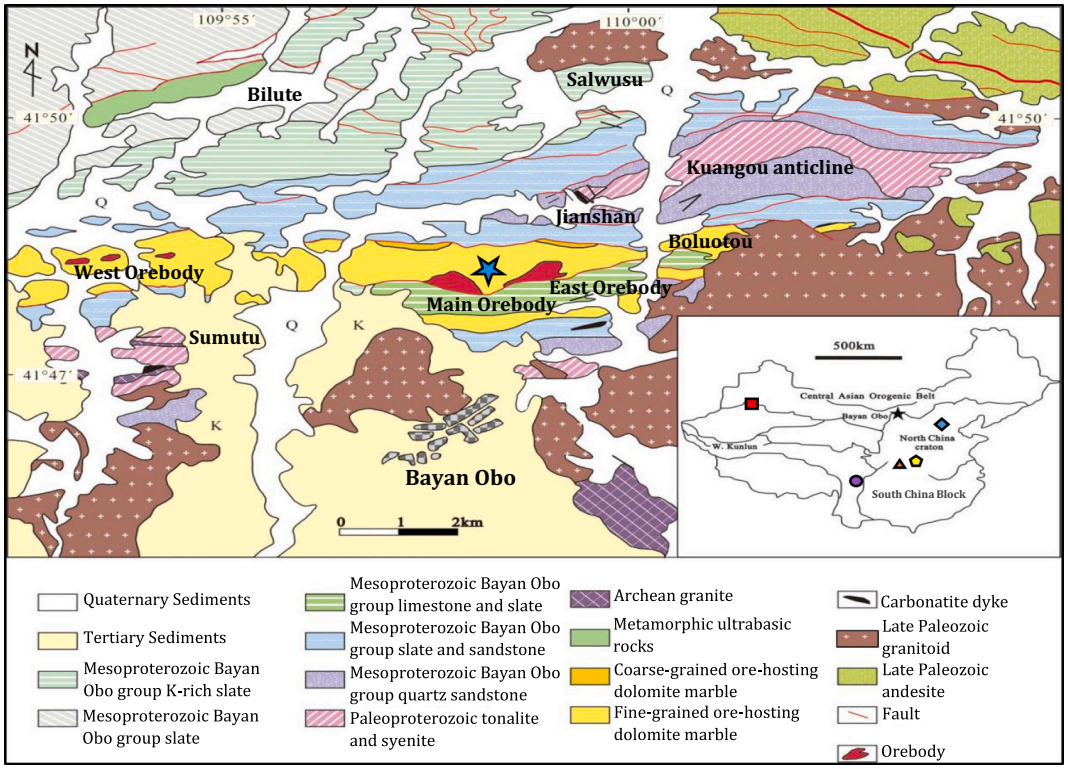

Fig. 1. Main diagram illustrates the geological map of the Bayan Obo district, northern China. Samples investigated here are from the host dolomitic marble of Mesoproterozoic Age (indicated by blue star). The inset displays the locations of Bayan Obo (star), Miaoya carbonatite complex (MCC; orange triangle), Maoniuping (purple circle), Huayangchuan (HYC; yellow pentagon), Qiganbulake mafic–ultramafic-carbonatite complex (QMC; red square) and Trans-North China Carbonatites (TNCC; blue diamond) within China. Modified after Yang et al. (2011) and Fan et al. (2016). (For interpretation of the references to colour in this figure legend, the reader is referred to the web version of this article.)

1997; Chen et al., 2020). The REE concentrations of H8 are generally ≥1 wt% classifying it as a REE ore deposit (Yang et al., 2017). The samples studied here are from a 1700 m drill core and thus have not been subjected to recent post-formation surface weathering or alteration processes.

3. Methods

3.1. Micro-XRF mapping

Qualitative chemical element maps (Ca, Ce, Fe, Mg, Mn, P, S, Si, Ti) for petrographic thin sections (~100 μm thick) of ten of the dolomite samples investigated here (1508, 1532, 1551, 1551.6, 1559, 1649.5, 1666, 1679, 1729, 1730) were obtained using an Edax Orbis micro-XRF instrument housed at the Center for Environmental Science and Technology (CEST), University of Notre Dame. The chemical element maps (Fig. 2; additional maps in supplementary information) were generated using a 30 μm beam overnight (~12 h) with an amplifier time of 12.8 μs and a fluorescent energy of 32 kV.

3.2. Microprobe analyses

Major and minor element concentrations (Table 1; Fig. 3) for minerals from nine of the carbonatites were determined by using a CAMECA SX-50 electron microprobe (EMP) at the University of Notre Dame. The EMP was operated with a 15 kV of accelerating voltage, 25 nA of beam current, and a beam diameter of 10 μm. The instrument was calibrated using the following standards per element; olivine (Fe, Mn), dolomite (Mg, Ca), and plagioclase (Sr). The peak and background counting times were 20 s for Mn and Fe, 10 s for Sr, Mg, and Ca. The raw k-ratios obtained were corrected using the CalcZAF program.

3.3. Trace element concentrations

Carbonate samples were processed for trace element abundance determinations (Table 2) in a class 1000 clean room laboratory at the Midwest Isotope and Trace Element Research Analytical Center (MITERAC), University of Notre Dame. Fragments (2–3 cm) obtained from varying depths of a 1700 m drill core were crushed, and carbonate fractions were subsequently hand-picked with the aid of a binocular microscope; the carbonate separates were then powdered by mortar and pestle. Several samples are from the same depth (meter) interval and indicated with a B (e.g., 1551 and 1551B), which are not duplicates and thus should be treated and discussed as separate samples. Approximately 50–60 mg of powder for each sample was digested in precleaned 15 mL Savillex® Teflon beakers using 4 mL of high purity 16 N HNO_3 overnight at room temperature. The digested samples were centrifuged and supernatants were subsequently diluted to ~50 mL with 18 MΩ cm^{-2} ultrapure water.

Trace element abundances were obtained using a Nu Plasma AttoM High Resolution Inductively Coupled Plasma Mass Spectrometer (HR-ICP-MS) in medium resolution mode ($M/\Delta M \approx 3000$) housed within MITERAC. The instrument's wet-plasma introduction system consists of a cyclonic spray chamber within a Peltier cooling device (at 7 °C), Meinhard nebulizer, and quartz torch. At the start of each analytical session, the instrument was tuned and calibrated with a multi-element 1 ppb standard solution. The concentrations of the trace elements were determined by a standard/spike addition method (Jenner et al., 1990), which includes corrections for matrix effects and instrumental drift.

3.4. Sr, Nd, Pb isotopes analyses

Sr, Nd, and Pb isotope ratio determinations were conducted subsequent to ion exchange chromatography on a Nu Plasma II Multi-

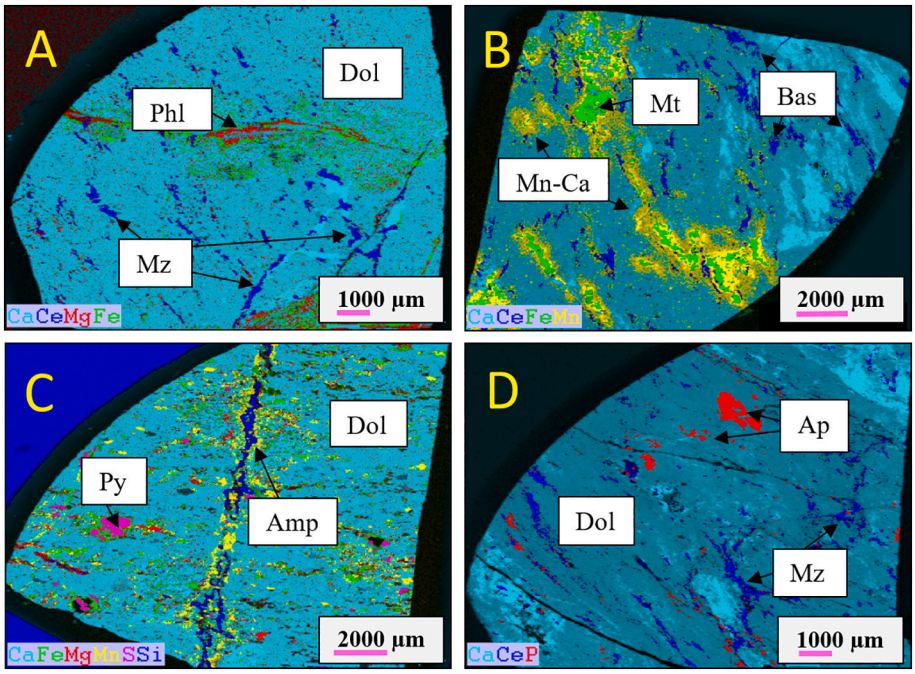

Fig. 2. Micro(µ)-XRF chemical element maps of several samples from Bayan Obo studied here. A. Sample 1551.6 shows distinct pockets of REE-bearing monazite-(Ce) (Mz) along fractures and a phlogopite vein (Phl) hosted by the predominant dolomite (Dol) matrix; B. Sample 1559 has magnetite (Mt) grains surrounded by Mn-rich carbonate (Mn−Ca) and significant bastnaesite inclusions (Bas); C. Sample 1679 contains pyrite (Py) and a vein of alkali-amphibole (Amp) within a dolomite matrix; D. Sample 1729 displays monazite-(Ce) pockets along with accessory apatite (Ap) crystals in a dolomite matrix.

Collector (MC) ICP-MS housed in MITERAC, which is equipped with a DSN-100 desolvating nebulizing system; a brief description of each separation chemistry is provided below.

All chemical separation methods employed the use of high purity acids produced in-house with the use of Savillex DST-1000, sub-boiling, acid purification systems. For separation of Sr, 13.4 cm ion exchange columns containing 4.3 mL of 200–400 mesh AG 50W-X8 resin were cleaned with 6 N HCl and 18 MΩ cm^{-2} ultrapure water and conditioned with high purity 2.5 N HCl. Purified Sr is eluted with high purity 2.5 N HCl, dried down, and brought back into ~2 mL of 2% HNO_3 for isotopic analysis. Strontium isotope measurements were conducted following the protocol outlined in Balboni et al. (2016). Strontium isotope data were acquired in static, multi-collection mode using 5 Faraday collectors for a total analysis time of 400 s. ^{85}Rb was monitored to correct for any isobaric overlap of ^{87}Rb with ^{87}Sr. The accuracy and reproducibility of the results were verified with repeated measurement of the NIST SRM 987 strontium isotope standard, which yielded an average value of 0.71025 ± 0.00004 (n = 4).

For purification of Nd, the rare earth elements (REEs) were first separated during the Sr ion exchange chemistry. They are eluted after Sr by using 6 N HCl. Subsequently, Nd was isolated from the REEs with 9.7 cm columns containing 1.22 mL 50–100 mesh Eichrom Ln-Spec resin. The resin is cleaned with 6 N HCl and conditioned with 0.18 N HCl while Nd is collected with 0.3 N HCl. Purified Nd aliquots were dried down and brought back into ~2 mL of 2% HNO_3 for analysis. Neodymium isotope data was acquired in static, multi-collector mode using seven Faraday collectors. Instrumental mass bias was corrected for using the $^{146}Nd/^{144}Nd$ ratio (0.7219) while accuracy and reproducibility were assessed via repeated measurements of the JNdi-1 standard (Tanaka et al., 2000; $^{143}Nd/^{144}Nd$ = 0.512115; n = 3).

For Pb separation, two sets of polypropylene columns fitted with a polystyrene frit filled with ~20 µL of 70–150 mesh Merck AG 1-X8 resin were used. The resin is cleaned with 18 MΩ cm^{-2} ultrapure water and 6 N HCl and conditioned with 0.8 N high purity HBr. Pb elutes with 6 N HCl and is dried down and then brought into 2% HNO_3 for analysis. Lead isotope data was collected following the protocol in Simonetti et al. (2004). The purified Pb aliquot is spiked with a NIST SRM 997 Thallium standard solution (5 ppb). The $^{205}Tl/^{203}Tl$ was measured in order to monitor instrumental mass bias (exponential law; $^{205}Tl/^{203}Tl$ = 2.3887), and ^{202}Hg was analyzed for the ^{204}Hg interference correction on ^{204}Pb. Data acquisition consists of a thirty-second on-peak zero on seven Faraday collectors followed by two blocks of 25 scans (10 s each). To ensure accuracy and reproducibility a 10 ppb solution of NIST SRM 981 Pb standard doped with NIST SRM 997 Tl was analyzed prior to the analytical session. Replicate measurements of the NIST SRM 997 Pb isotope standard (n = 4) yielded the following average Pb isotope ratios; $^{206}Pb/^{204}Pb$ = 16.935 ± 0.003, $^{207}Pb/^{204}Pb$ = 15.488 ± 0.002, $^{208}Pb/^{204}Pb$ = 36.686 ± 0.008.

3.5. $\delta^{13}C$ and $\delta^{18}O$ compositions

Carbon and oxygen isotope analyses were conducted in the Center for Environmental Science and Technology (CEST) at the University of Notre Dame. The powdered carbonate fraction (200–300 µg) of each sample was digested using the conventional orthophosphoric acid method involving ~0.2 mL concentrated H_3PO_4 in sealed tubes at room temperature (25 °C) for 24 h (McCrea, 1950). The sample gas was flushed with He into a Delta V with Thermo Gasbench Isotope Ratio Mass Spectrometer for isotopic analysis. Carbon and oxygen isotope ratios are reported in per mil notation (‰) relative to Peedee Belemnite (PDB; Craig, 1957) for $\delta^{13}C$ and standard mean oceanic water (SMOW; Coplen et al., 1983) for $\delta^{18}O$. Three external limestone standards (NBS 19, YWCC, RoyCC) were used to ensure the accuracy of the $\delta^{13}C$ and $\delta^{18}O$ results obtained.

3.6. Boron concentrations

Boron abundances of the samples investigated here were obtained via solution-(wet plasma) mode analysis using the same Nu Plasma AttoM HR-ICP-MS instrument described earlier. Sample powders (50–60 mg) were digested at room temperature in concentrated high purity HNO_3 acid and subsequently diluted to a volume of 50 mL with 18 MΩ cm^{-2} ultrapure water. Indium was used as an internal standard to monitor and correct for instrument drift and matrix effects. Boron contents were calculated based on an external calibration technique using a certified boron elemental standard solution (NIST SRM 3107; certified concentration of 999.2 ppm).

Table 1
Major and minor elemental abundances (wt.%) of select samples from Bayan Obo

Sample/point	MgO	FeO	MnO	CaO	SrO	SUM
1508-1	16.14	5.73	1.66	28.19	0.14	51.86
1508-2	14.60	7.86	1.80	28.35	0.17	52.77
1508-3	14.75	7.53	1.59	28.37	0.19	52.43
1508-4	13.83	8.46	1.79	28.14	0.19	52.41
1508-5	14.40	8.18	1.73	28.08	0.03	52.42
1532-1	15.08	7.52	1.62	27.73	0.24	52.19
1532-2	14.78	7.35	1.82	28.17	0.27	52.39
1532-3	15.79	6.42	1.90	27.65	0.26	52.01
1532-4	14.75	7.75	1.77	27.89	0.18	52.35
1532-5	15.13	7.27	2.00	28.07	0.28	52.74
1532-6	16.01	6.48	1.98	27.63	0.36	52.47
1532-7	15.97	6.34	2.04	27.90	0.26	52.50
1532-8	15.96	6.41	1.97	28.32	0.29	52.96
1551-1	14.80	7.46	1.69	28.68	0.35	52.97
1551-2	14.91	6.31	1.73	28.24	0.20	51.40
1551-3	15.36	7.04	1.45	28.66	0.25	52.77
1551-4	14.87	7.41	1.60	28.16	0.22	52.26
1551-5	16.18	6.25	1.52	27.99	0.33	52.28
1551-6	15.30	7.17	1.62	27.95	0.27	52.31
1551-7	15.39	7.37	1.59	27.80	0.30	52.46
1551-8	15.31	7.73	1.62	27.97	0.29	52.92
1551.6-1	15.92	6.08	1.49	28.10	0.23	51.81
1551.6-2	15.34	6.99	1.60	28.08	0.27	52.27
1551.6-3	15.37	6.41	1.68	28.38	0.33	52.18
1551.6-4	14.74	7.17	1.80	28.74	0.27	52.72
1551.6-5	16.20	5.91	1.19	28.25	0.27	51.82
1551.6-6	14.91	7.05	1.88	28.66	0.16	52.66
1559-1	15.96	5.67	1.55	28.03	0.31	51.52
1559-2	15.31	6.68	1.83	28.13	0.26	52.22
1559-3	14.87	7.49	1.62	28.15	0.31	52.45
1559-4	16.32	5.92	1.45	28.04	0.33	52.06
1559-5	14.41	8.98	1.92	28.19	0.12	53.63
1649.5-1	16.44	5.64	1.25	28.06	0.44	51.84
1649.5-2	16.95	5.30	1.09	27.61	0.45	51.39
1649.5-3	15.98	6.33	1.63	27.95	0.42	52.30
1649.5-4	15.87	6.48	1.69	28.13	0.40	52.57
1649.5-5	15.60	6.71	1.71	27.71	0.34	52.06
1649.5-6	15.64	6.45	1.65	28.32	0.30	52.36
1649.5-7	15.79	6.10	1.60	28.06	0.40	51.95
1649.5-8	15.70	6.54	1.55	27.94	0.44	52.17
1666-1	15.09	6.88	1.50	28.18	0.46	52.12
1666-2	15.03	6.72	1.37	27.97	0.46	51.55
1666-3	15.45	6.51	1.37	28.10	0.59	52.03
1666-4	16.03	6.12	1.39	27.49	0.53	51.55
1666-5	15.52	6.02	1.39	27.74	0.65	51.32
1729-1	13.81	9.19	1.60	27.73	0.41	52.75
1729-2	15.01	7.54	1.33	27.67	0.46	52.01
1729-3	15.65	7.14	0.83	28.37	0.39	52.38
1729-4	14.50	8.23	1.57	27.89	0.49	52.68
1729-5	14.21	8.38	2.10	27.57	0.33	52.59
1730-1	14.58	9.13	2.11	27.01	0.32	53.14
1730-2	15.54	7.23	1.73	27.41	0.26	52.18
1730-3	15.20	7.79	1.75	27.47	0.25	52.47
1730-4	15.09	7.62	1.92	27.42	0.25	52.30
1730-5	14.93	7.75	1.90	27.53	0.22	52.32
1730-6	14.88	8.04	1.99	27.13	0.33	52.36
1730-7	13.91	9.57	2.17	26.93	0.31	52.89

3.7. In-situ, semi-quantitative assessment of boron distribution

High spatial resolution analyses obtained by laser ablation (LA)-ICP-MS were conducted in order to better evaluate the boron isotope compositions for the Bayan Obo carbonates reported here (Table 3). In particular, the analytical goals were to determine: 1- boron abundances in the different phases present within individual Bayan Obo samples, 2- boron contents within different textural areas of individual samples, and 3- boron concentrations for samples with either contrasting petrographic characteristics and/or $\delta^{11}B$ values. Due to the lack of an appropriate matrix-matched external standard, the absolute (ppm) boron concentrations cannot be calculated as with standard laser ablation analyses; however, the relative differences (if present) in recorded ion signal intensities may serve as an effective proxy for comparing relative boron concentrations at the 100's of micron scale within selected samples.

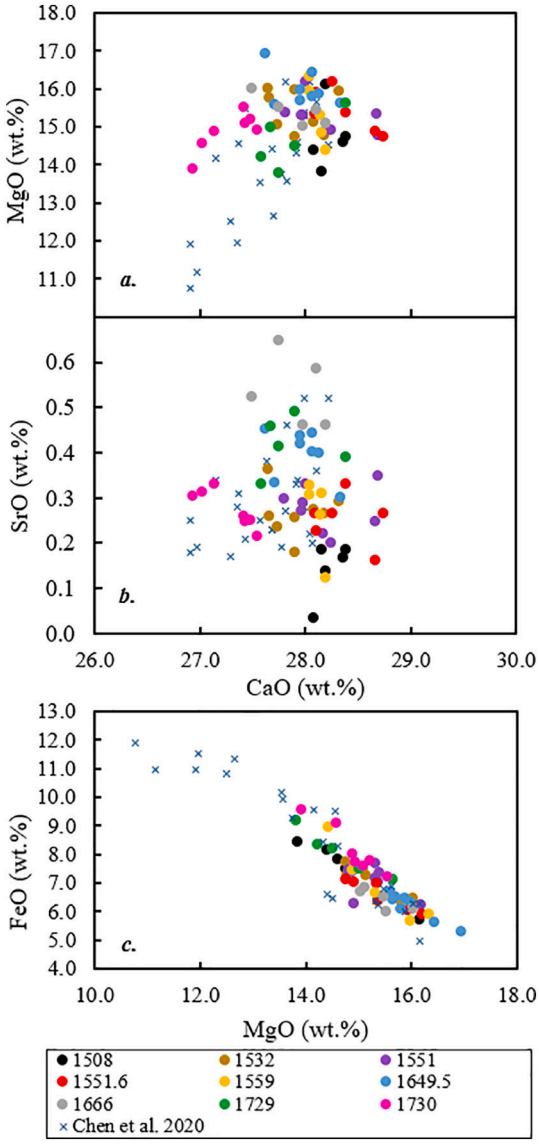

Fig. 3. Major and minor element compositions obtained by electron microprobe analyses for carbonates from the Bayan Obo ore-bearing host body. (a) MgO (wt %) and (b) SrO (wt%) vs. CaO (wt%), (c) FeO (wt%) vs. MgO (wt%). These are compared to compositional data for Bayan Obo dolomite samples from Chen et al. (2020).

Semi-quantitative assessment of the in-situ boron abundances for the Bayan Obo samples were obtained by laser ablation-ICP analysis during a single day of analysis using a New Wave Research UP213 Nd:YAG laser system coupled to the same Nu Plasma Attom HR-ICP-MS described above. Both single spot and raster analyses were performed using a spot size of 250 μm with a 2 Hz repetition rate resulting in an energy density of ~2 J/cm^2. Prior to analysis, the ^{11}B background signal was measured for ~60 s with the laser on and shuttered. The instrument was tuned for maximum boron ion signal and monitored throughout the analytical session using the NIST SRM 610 glass wafer (B = 351 ppm) as the reference material, which gave a median ^{11}B ion signal of 453,400 ± 124,000 (2σ level) counts per second (cps) (n = 7 analyses). This corresponds to an approximate ion yield of 1300 cps/ppm for ^{11}B, and provides a rough estimate of the expected B ion signal

Table 2
Trace element concentrations (ppm) in Bayan Obo samples.

	1508	1508B	1559	1559B	1729	1729B	1730	1649.5	1666	1666B	1679	1679B	1532	1551	1551B	1551.6
	FG	FG	FG	FG	FG	FG	FG	CG	CG	CG	CG	CG	HG	HG	HG	HG
B	1.06	0.69	0.40	0.58	0.55	0.86	0.92	1.14	0.42	0.78	0.56	0.76	0.82	0.60	0.78	0.89
Sc	38.5	23.6	6.9	22.6	4.4	10.2	7.8	18.2	16.9	30.1	20.4	20.3	13.1	10.2	21.4	33.1
V	7.4	5.4	14.5	7.1	7.6	4.2	0.7	6.2	9.1	12.7	2.9	6.3	2.1	2.4	3.1	4.2
Cr	0.6	1.5	0.3	0.8	2.9	0.0	bdl	0.3	0.6	1.0	0.7	1.4	0.7	0.4	0.6	0.1
Co	7.7	2.5	1.1	4.7	9.0	3.8	0.2	4.0	3.1	5.2	13.5	11.4	1.8	1.0	5.6	7.9
Ni	2.8	1.8	1.6	2.1	1.5	0.8	0.5	1.1	2.3	1.1	2.9	3.0	2.4	1.7	1.9	2.0
Cu	0.6	bdl	0.6	bdl	1.0	bdl	bdl	bdl	0.6	bdl	1.4	8.1	bdl	0.6	bdl	bdl
Zn	64.6	60.8	180	96.3	1688	329	30.0	305	54.1	67.1	65.7	125	70.0	3.7	149	202
Rb	0.0	0.0	0.6	2.2	0.7	0.8	0.7	0.0	0.4	0.0	0.0	0.0	0.3	1.9	2.3	0.7
Sr	1100	1252	1552	629	1118	1012	432	1600	2754	1472	1286	1692	1712	1215	545	1193
Y	42.9	43.4	106	46.2	52.9	36.0	21.7	71.9	70.7	89.8	98.5	83.5	62.6	227	50.7	124
Zr	0.1	0.3	0.1	0.6	0.1	0.2	0.2	0.1	0.1	0.1	0.0	0.0	0.1	0.1	0.1	0.2
Nb	1.2	10.3	3.3	32.2	27.4	12.8	29.1	0.5	3.9	1.7	0.4	2.7	7.9	2.9	4.3	5.8
Mo	2.0	0.7	0.4	0.6	6.8	0.7	0.0	1.1	4.0	2.5	0.7	4.3	1.4	4.7	0.8	1.8
Cs	0.0	0.0	0.0	0.0	0.1	0.1	0.0	0.0	0.0	0.0	0.0	0.3	0.0	0.1	0.1	0.0
Ba	444	1000	293	421	443	437	568	372	273	650	99.3	67.0	39.6	99.5	407	777
La	761	1123	1167	317	1134	357	573	509	712	1299	410	208	473	564	208	1017
Ce	932	1501	1594	720	1898	744	888	892	474	1623	489	302	503	1108	369	1151
Pr	83.7	135	150	74.9	191	91.5	87.3	119	44.6	144	50.0	32.6	46.9	139	38.2	116
Nd	257	418	500	246	674	367	282	538	141	487	194	110	156	594	134	431
Sm	18.3	36.4	111	16.6	64.6	31.5	23.0	58.5	29.6	50.6	18.5	15.9	20.3	100	19.4	53.6
Eu	5.9	7.6	12.6	4.7	10.9	10.4	6.9	14.9	4.5	18.3	8.8	7.4	5.8	43.3	5.6	15.5
Gd	13.1	18.6	41.0	12.6	25.8	19.5	15.1	32.8	13.8	33.8	24.0	15.2	15.2	104	14.9	37.5
Tb	1.6	1.6	5.5	2.1	2.2	1.7	1.4	3.8	1.9	4.1	4.4	2.5	2.1	14.5	2.1	4.9
Dy	7.3	6.5	25.2	12.4	8.5	7.8	6.1	15.8	9.1	18.5	23.4	14.7	10.5	66.2	11.9	24.1
Ho	1.4	1.1	3.8	2.3	1.4	1.3	0.9	2.3	1.5	2.7	3.7	2.4	1.7	9.5	2.2	3.8
Er	3.1	2.2	7.5	5.6	3.0	2.9	2.0	4.1	2.9	5.3	6.8	4.8	3.8	16.9	4.8	7.3
Tm	0.3	0.2	0.6	0.6	0.4	0.3	0.2	0.3	0.2	0.4	0.6	0.4	0.4	1.5	0.4	0.7
Yb	1.9	1.4	2.7	2.7	1.8	1.5	1.1	1.6	1.1	2.1	2.4	1.7	1.7	5.4	2.2	2.9
Lu	0.2	0.1	0.2	0.2	0.2	0.2	0.1	0.1	0.1	0.2	0.2	0.1	0.2	0.5	0.2	0.3
W	0.1	0.1	0.1	0.4	0.2	0.1	0.2	0.1	0.1	0.1	0.1	0.1	0.4	0.2	0.1	0.1
Pb	22.3	33.4	114	41.6	287	202	78.3	35.1	27.9	101	66.6	137	12.9	27.6	14.7	34.7
Th	4.5	6.9	2.6	6.5	25.8	2.0	2.4	1.4	1.1	0.6	0.4	0.3	2.7	2.1	2.5	11.3
U	0.08	0.07	0.38	0.05	0.62	0.71	0.06	0.06	0.04	0.02	0.03	0.01	0.24	0.03	0.03	0.14
LREE	2053	3214	3522	1375	3962	1591	1854	2118	1402	3603	1161	668	1199	2506	769	2769
TREE	2088	3253	3621	1418	4016	1637	1888	2193	1437	3688	1236	717	1240	2768	814	2866

bdl = below detection limit; LREEs = sum of light rare earth elements (La to Sm); TREEs = total of all rare earth element abundances. FG = fine-grained dolomite matrix; CG = coarse-grained dolomite matrix; HG = heterogeneous-grained (mixed) dolomite matrix.

Table 3
Carbon, oxygen, and boron isotope data from Bayan Obo carbonates.

Sample	Type	$\delta^{13}C$ (‰)	Uncertainty	$\delta^{18}O$ (‰)	Uncertainty	$\delta^{11}B$[a] (‰)
1508	FG	-2.3	0.1	12.4	0.1	-6.5
1508B	FG	-1.7	0.1	13.7	0.2	-3.8
1559	FG	0.6	0.1	14.5	0.1	-6.2
1559B	FG	-0.1	0.1	14.5	0.1	-1.0
1729	FG	-0.6	0.1	12.1	0.1	-14.5
1729B	FG	0.5	0.1	12.9	0.1	-7.8
1730	FG	0.8	0.1	12.7	0.2	6.4
1649.5	CG	-0.9	0.0	14.0	0.1	-7.9
1666	CG	-0.6	0.1	13.7	0.1	-9.0
1666B	CG	0.1	0.1	14.3	0.1	-3.6
1679	CG	0.1	0.1	14.3	0.1	-7.6
1679B	CG	-0.4	0.1	13.4	0.1	-8.6
1532	HG	-1.6	0.1	13.9	0.2	-3.4
1551	HG	-0.2	0.1	13.6	0.1	-7.1
1551B	HG	-1.2	0.0	13.8	0.1	-1.9
1551.6	HG	-1.8	0.1	13.8	0.1	-5.2

[a] $\delta^{11}B$ associated uncertainty (± 0.5‰) based on replicate analyses of in-house coral standard

for the Bayan Obo dolomite samples (≤1 ppm; Table 2), while also taking into account the difference in sample matrices being ablated (silicate vs. carbonate).

3.8. $\delta^{11}B$ compositions

Procedures for boron isotope analyses were adapted from Hulett et al. (2016). Sample powders (0.1–0.25 g) were digested in concentrated HNO_3 and dried down at 95 °C. Subsequent to digestion, samples were purified by ion-exchange column chemistry using a 1 mL pipette tip filled with ~250 µL of the B-specific Amberlite IRA-743 resin pre-cleaned with 2% HNO_3. Isotope ratio measurements of the purified B sample aliquots (~100 ng total B) were determined via solution-mode on a Nu Plasma II multi-collector-ICP-MS housed within MITERAC. Each analysis consisted of a 30 s on-peak zero cycle followed by a two-minute analysis cycle involving simultaneous measurement of ^{10}B and ^{11}B ion signals on Faraday collectors. To minimize background B ion signals, a boron-free, wet plasma introduction system was used, which consisted of a PFA nebulizer, PFA spray chamber (housed within a peltier cooling device @7 °C), and demountable quartz torch equipped with a sapphire injector. Aliquots (~0.003 g) of a modern coral standard ($\delta^{11}B$ = +23‰) obtained from Dr. Troy Rasbury at Stony Brook University were repeatedly digested, and underwent the same ion exchange chemistry with each batch of samples so as to validate the B isotope results obtained; the calculated average $\delta^{11}B$ value and associated standard deviation is +23.2 ± 0.5‰ (13 replicates), which agrees with the recommended value cited above. In addition, sample-standard bracketing employing a ~ 100 ppb solution of the NIST SRM 951a boron isotope standard was used to correct for instrument drift and ensure acceptable reproducibility, typically < 0.5‰ (2σ level) per analytical session; the NIST SRM 951a solution typically yielded ~0.7 V

ion signal of ^{11}B. Boron isotope results are reported as averages of several duplicate runs with acceptable reproducibility (e.g., 1508; −6.9 and −6.1‰) using the conventional $\delta^{11}B$ (‰) notation (e.g., Hulett et al., 2016). Replicate analyses of samples were not always performed on the same day.

4. Results

4.1. Petrography and major and trace element geochemistry

Several of the μ-XRF chemical element maps produced for samples studied here (Fig. 2; additional maps found in supplementary information) display the dominant dolomitic carbonate matrix along with accessory minerals (e.g., bastnaesite, monazite, apatite, phlogopite, pyrite) reported previously for Bayan Obo's host ore body (Smith et al., 2015 and references therein). Detailed mineralogical and petrological studies of the Bayan Obo carbonatite have documented over 170 named minerals including both 20 REE- and Nd-bearing minerals (Chao et al., 1995; Zhang et al., 1996; Smith et al., 2015; Fan et al., 2016; Yang et al., 2017; Liu et al., 2018a; Ren et al., 2019). Smith et al. (2015) and Liu et al. (2018a) proposed that the complex mineralogy of the Bayan Obo dolomitic marble formed via a multi-stage paragenetic sequence where the earliest minerals to crystallize include dolomite, calcite, apatite, limited quartz, albite, and zircon cores. Notably, Smith et al. (2015) stated that the earliest phase of REE mineralization involved monazite-(Ce) intergrown with ferroan dolomite developing along grain boundaries and fractures within the marble. This texture is visible in the μ-XRF maps for samples 1551.6 and 1729 where monazite-(Ce) grains occupy fractures in the host dolomite (Fig. 2a, d). Proposed secondary paragenetic stages include the formation of apatite, magnetite (one of the main Fe-bearing minerals), fluorite, and alkali-amphiboles, such as aegirine and riebeckite (Fig. 2b, c; Smith et al., 2015; Liu et al., 2018a, 2018b; Ren et al., 2019). Of importance, Chen et al. (2020) noted significant intra-sample variability of the Bayan Obo host dolomite both in relation to the trace element contents and radiogenic isotope compositions, which correlate to the dominant grain size of carbonate within the sample. Specifically, Chen et al. (2020) categorized the dolomite into three facies; fine-grained (FG: 1508, 1508B, 1559, 1559B, 1729, 1729B, 1730), coarse-grained (CG: 1649.5, 1666, 1666B, 1679, 1679B) and heterogeneous (HG: 1532, 1551, 1551B, 1551.6); a distinction recognized and used in this study. The major and minor element compositions for nine of the samples investigated here are listed in Table 1 and illustrated in Fig. 3. The MgO and CaO wt% concentrations are consistent with carbonates of dolomitic compositions (13.81–16.95% and 26.93–28.74%, respectively; Table 1), and these overlap with previously reported Bayan Obo host dolomite values (Ren et al., 2019; Chen et al., 2020). All of the dolomite samples are ferroan in composition (5.30–9.57 wt% FeO) with SrO concentrations varying between 0.03 and 0.65 wt%.

Trace element and boron concentrations for carbonate separates examined here are reported in Table 2. Of note, the hand-picked separates may not consist of entirely 100% carbonate as micron-sized inclusions of other minerals, in particular REE-bearing phases (e.g., apatite, monazite) may be present, and their presence may bias the exact REE abundances in the sample aliquots investigated here. This is evident in Fig. 4 which compares the REE abundances obtained here to concentrations reported for bulk rock (solution mode-ICP-MS) digestions and in-situ, high spatial resolution analyses (laser ablation-ICP-MS) of dolomite grains from Bayan Obo (both from Chen et al., 2020). The results displayed in Fig. 4 indicate chondrite normalized REE patterns consistent with those reported in previous work (Chen et al., 2020), and as expected, plot between the data for bulk rock digestions and in-situ analyses. The former will always yield the highest concentrations as REE-bearing phases are also digested in the solution mode, whole rock analyses (gray field in Fig. 4), and the latter will have the lowest contents as these are micron-scale investigations of solely the dolomite matrix (purple field in Fig. 4). The total rare earth element (TREE) concentrations of the sample powders studied here vary between 717 and 4016 ppm, and the corresponding chondrite-normalized (CN)-REE patterns (Fig. 4) show light rare earth element (LREE) enrichment ($La/Lu_{(CN)}$ = 94–950). Of note, sample 1551 has higher concentrations of heavy REEs (HREEs; Eu to Ho), which may be due to the documented trace element variability within the Bayan Obo host dolomite (Chen et al., 2020). For example, 1551B is taken from the same drill core depth as 1551, but is characterized by a significantly lower TREE content (~1900 ppm).

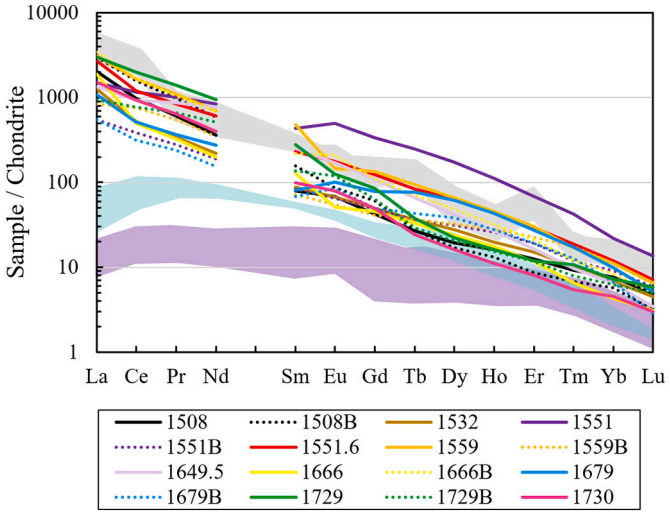

Fig. 4. Chondrite-normalized REE patterns for samples from Bayan Obo (solid and dotted lines) analyzed in this study compared to 1. Solution mode, whole rock samples for Bayan Obo host dolomite (gray shaded region), 2. In-situ coarse-grained dolomite grains (teal shaded field), and 3. In-situ fine-grained dolomite grains (purple shaded field) from Chen et al. (2020). Chondrite data are from Sun and McDonough (1989). (For interpretation of the references to colour in this figure legend, the reader is referred to the web version of this article.)

Additionally, the abundances for the remaining trace elements for the samples analyzed here (Table 2) in general overlap with published results for Bayan Obo's host dolomite (Yang et al., 2011; Chen et al., 2020). The boron concentrations reported here are ≤1 ppm, which fall within the range defined for both unaltered (fresh) and high-temperature altered mid-ocean ridge basalts (MORBs; Spivack and Edmond, 1987; Ishikawa and Nakamura, 1992; Marschall et al., 2017). These B abundances are also consistent with a vast majority of reported boron concentrations for carbonatites worldwide (Hulett et al., 2016; Çimen et al., 2018, 2019), and are markedly lower than those for bulk continental crust (average = 10 ppm; Marschall et al., 2017) and the range for carbonate sediments (13–26 ppm; Ishikawa and Nakamura, 1993).

4.2. Boron, carbon, and oxygen isotope data

Oxygen and carbon stable isotope data obtained for carbonates examined here are listed in Table 3 and illustrated in Figs. 5 and 6. Fig. 5a displays the oxygen isotopic compositions of the Bayan Obo samples with their corresponding LREE contents compared to those for carbonate separates from Miaoya carbonatite complex (MCC; Çimen et al., 2018). Fig. 6 includes a comparison of the C and O isotope results obtained here to those for carbonates from the MCC (Çimen et al., 2018). The $\delta^{18}O_{SMOW}$ (‰) and $\delta^{13}C_{PDB}$ (‰) values for the Bayan Obo samples vary between +12.1 and +14.5 ‰ and -2.3 and 0.8 ‰, respectively, and do not plot within the field for "primary igneous carbonatites (PIC)" ($\delta^{18}O_{SMOW}$ ~ +6 to +10 ‰ and $\delta^{13}C_{PDB}$ ~ -4 to -8 ‰; Keller and Hoefs, 1995; Fig. 6a). All of the samples analyzed in this study plot above and to the right of the PIC box. Additionally, the $\delta^{18}O_{SMOW}$ and

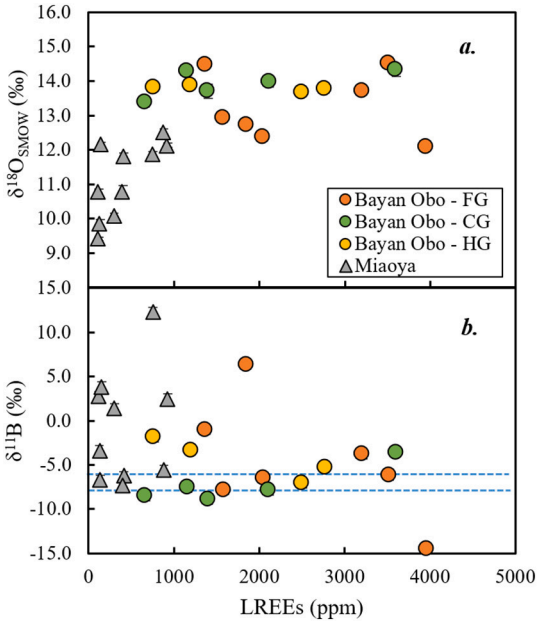

Fig. 5. (a) $\delta^{18}O_{SMOW}$ and (b) $\delta^{11}B$ values vs. LREE abundances for Bayan Obo samples investigated here compared to those reported for carbonates from Miaoya carbonatite complex (Çimen et al., 2018). Each type of carbonate from Bayan Obo is colour coded; fine-grained (FG; orange), coarse-grained (CG; green), and heterogeneous (HG; yellow). (b) Asthenospheric mantle boron isotopic composition field (−7.1 ± 0.9‰; Marschall et al., 2017) indicated with dashed blue lines. Associated analytical uncertainty, where not visible, is within the size of the symbol. (For interpretation of the references to colour in this figure legend, the reader is referred to the web version of this article.)

$\delta^{13}C_{PDB}$ values for the Bayan Obo samples overlap with previously documented C and O isotope compositions for Bayan Obo's host dolomitic marble, but differ from those of carbonatite dolomites or sedimentary dolomites (Fig. 6a; Le Bas et al., 1997; Smith et al., 2015). The $\delta^{13}C_{PDB}$ and $\delta^{18}O_{SMOW}$ values for the Bayan Obo carbonates do not plot along a unique Rayleigh fractional crystallization line (Fig. 6a; after Deines, 1989).

The first-reported boron isotopic compositions ($\delta^{11}B$) for the Bayan Obo carbonates analyzed here are listed in Table 3 and define a total range of values between -14.5 and +6.4 ‰. Samples consisting of fine-grained (FG) dolomite exhibit the greatest range of $\delta^{11}B$ values (−14.5 to +6.4‰; Table 3); specifically, sample 1729 (FG) yields the most depleted $\delta^{11}B$ value (−14.5‰), compared to MORB, whereas another fine-grained dolomite sample (1730) is characterized by the heaviest $\delta^{11}B$ value (+6.4‰; Table 3). In contrast, the range of values for samples containing coarse-grained (CG; −9.0 to −3.6‰) and heterogeneous-grained (HG) dolomite (−7.1 to −1.9‰; Table 3) are less variable. Moreover, there is no correlation between boron isotope compositions and their corresponding B concentrations (not shown). Fig. 5b also illustrates a lack of correlation between $\delta^{11}B$ signatures with corresponding total LREE concentrations. Eight of the carbonates record $\delta^{11}B$ compositions that are within uncertainty of the accepted value for asthenospheric MORB mantle (−7.1 ± 0.9‰; Marschall et al., 2017) independent of their C and O isotope compositions and TREE contents (Figs. 5 and 6). Of importance, there is significant variation in the $\delta^{11}B$ values reported for carbonate samples taken at the same depth interval within the core, with several pairs indicating as much as 5‰ difference for all three types (FG, CG, HG) of dolomite matrix (Table 3); there is only one pair (1679 and 1679B) that yields $\delta^{11}B$ values within the reported analytical uncertainty (−7.6‰ and − 8.6‰; Table 3). The boron isotope data are compared with their corresponding oxygen, carbon, and Sr isotope compositions in Figs. 6 and 7. Fig. 7a shows a negative trend between Sr contents and $\delta^{11}B$ values.

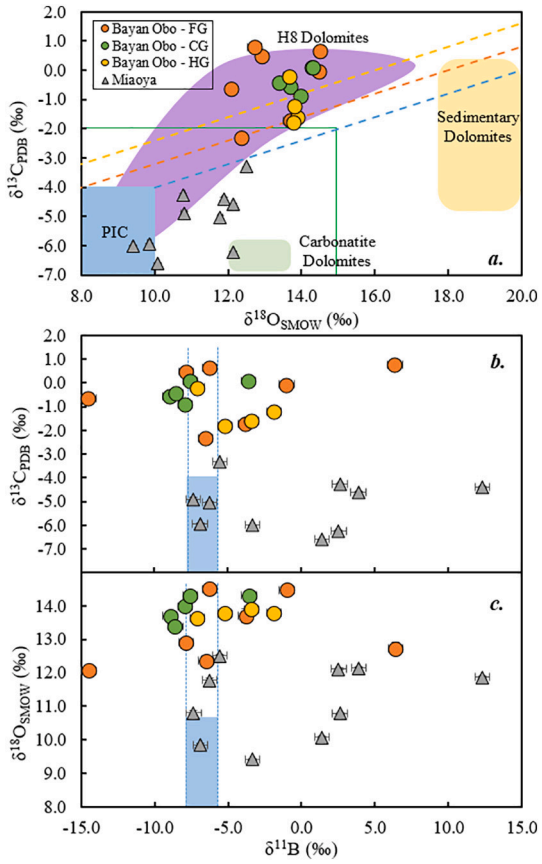

Fig. 6. Oxygen, carbon, and boron isotopic compositions for samples from Bayan Obo (this study) and Miaoya (Çimen et al., 2018). (a) $\delta^{13}C_{PDB}$ (‰) vs. $\delta^{18}O_{SMOW}$ (‰) with blue shaded area indicating the "Primary Igneous Carbonatite (PIC)" field (Keller and Hoefs, 1995). The green outline shows the range of C and O isotope compositions compatible with closed-system fractional crystallization, and the dashed lines represent Rayleigh fractional crystallization lines (m = 0.4) of carbonatites adopting different initial C and O isotope values within the PIC (after Deines, 1989). The purple shaded field encompasses C and O isotope values for the Bayan Obo host dolomite from previous studies (Le Bas et al., 1997; Smith et al., 2015). Other shaded regions indicate sedimentary (yellow) and carbonatite (green) dolomites from Smith et al. (2015). (b) $\delta^{13}C_{PDB}$ (‰) and (c) $\delta^{18}O_{SMOW}$ (‰) vs. $\delta^{11}B$ (‰) with shaded area corresponding to the PIC field and asthenospheric (MORB) $\delta^{11}B$ values (Marschall et al., 2017). Dashed blue lines indicate an extension of the latter field to heavier C and O isotope values. Associated uncertainties, where not visible, are within the size of the symbol. (For interpretation of the references to colour in this figure legend, the reader is referred to the web version of this article.)

4.3. Radiogenic (Sr, Nd, Pb) isotope data

The Sr, Nd, and Pb isotopic compositions for the samples analyzed here are listed in Tables 4, 5a and 5b, and illustrated in Figs. 7 and 8, and these are compared to those reported for carbonates from the Miaoya carbonatite complex (MCC; Çimen et al., 2018). Although a single stage isotopic evolution of Bayan Obo may be inadequate to describe the complexity of the protracted mineralization, a single emplacement age of 1.3 Ga (Smith et al., 2015) is adopted here for calculation of initial Sr, Nd, and Pb isotope ratios; the latter will be used to characterize any possible inherited isotopic signatures of the mantle source. The dolomitic carbonate samples record low $^{87}Rb/^{86}Sr$ values (0.00004–0.013) resulting in minimal age-decay corrections to measured $^{87}Sr/^{86}Sr$ values yielding two groups of initial values;

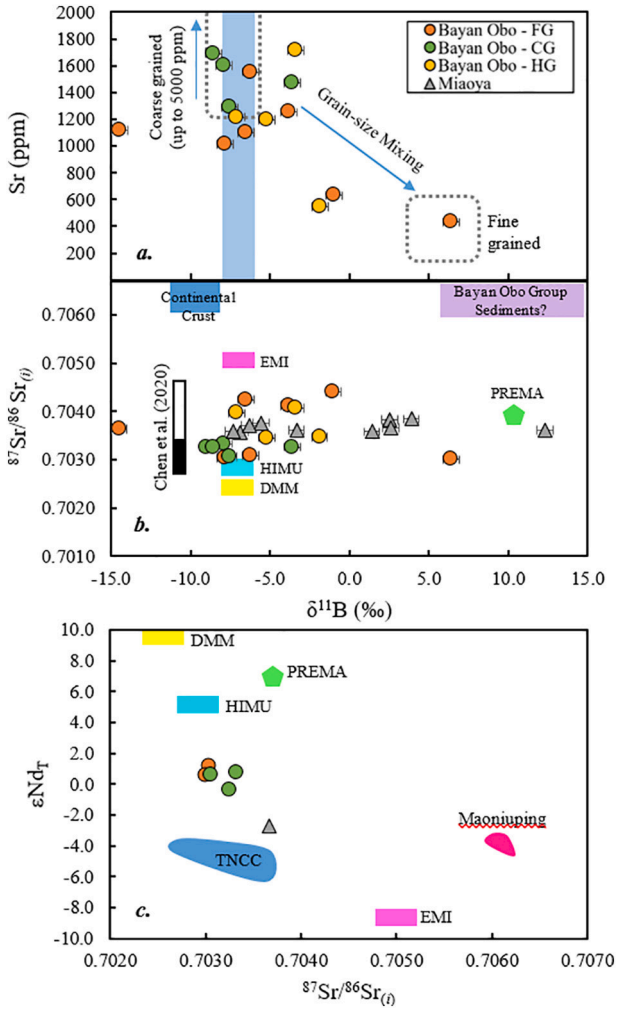

Fig. 7. (a) Strontium concentrations and (b) strontium isotopic ratios vs. $\delta^{11}B$ compositions for all samples from Bayan Obo (this study). (c) $\varepsilon Nd_{(t)}$ vs. initial $^{87}Sr/^{86}Sr$ values for pristine samples of dolomite from Bayan Obo. (a) Fields for coarse- and fine-grained dolomite, as described in Chen et al. (2020), are outlined with gray dashed rectangles. The blue field represents the $\delta^{11}B$ composition for asthenospheric mantle (Marschall et al., 2017). (b) Previously reported range of initial Sr isotope values for H8 dolomite (white rectangle) and 'pristine' coarse-grained H8 dolomite (black rectangle; Chen et al., 2020) are plotted. Sr and Nd isotope compositions for HIMU, EMI, and DMM fields are from Zindler and Hart (1986), and their corresponding $\delta^{11}B$ values are assumed to be that of asthenospheric MORB-like mantle (Marschall et al., 2017). Data for PREMA-like mantle fluid component is from Dixon et al. (2017). Estimated field for Bayan Obo Group sediments (purple) is plotted. Sources for the other data are from previous studies: Miaoya (Çimen et al., 2018); Trans-North China Carbonatites (TNCC; blue; Xu et al., 2019), Maoniuping (pink; Xu et al., 2003). Associated uncertainties are within the size of the symbol. (For interpretation of the references to colour in this figure legend, the reader is referred to the web version of this article.)

0.70300–0.70333 and 0.70345–0.70441 (Table 4). These overlap with previously reported values for the host dolomitic marble (Le Bas et al., 1997; Smith et al., 2015; Chen et al., 2020). The two groups of Sr isotopic compositions closely align with the Chen et al. (2020) bimodal classification of dolomite facies from Bayan Obo based on their $^{87}Sr/^{86}Sr_{(i)}$ values; coarse-grained samples are characterized by $^{87}Sr/^{86}Sr$ ratios of 0.70295–0.70314, whereas fine-grained/heterogeneous samples record ratios of 0.7032–0.70465. Corresponding Rb–Sr and Sm–Nd isochron plots (not shown) yield errorchrons (i.e., associated with significant uncertainties) with corresponding ages of ~2.7 Ga and ~397 Ma, respectively. The latter may be attributed to resetting of this isotope system due to Caledonian metasomatic events (~450 Ma; Smith et al., 2015). The $^{147}Sm/^{144}Nd$ ratios vary between 0.044 and 0.117 resulting in calculated initial $^{143}Nd/^{144}Nd$ ratios of 0.51053 to 0.51113. Eight of the calculated initial εNd_{CHUR} values based on this Mesoproterozoic age define a range of −1.5 to 1.2 similar to previously reported values for the Bayan Obo host dolomite (Smith et al., 2015). However, samples 1532, 1551, 1551B, 1551.6, 1559, 1666, and 1679B have more negative εNd_{CHUR} values (−3.0 to −12.6), which overlap with those documented for mineral separates from Bayan Obo (e.g., aegerine, aeschynite-(Ce), apatite, monazite; Nakai et al., 1989; Philpotts et al., 1991; Wang et al., 1994; Song et al., 2018) and is discussed in more detail below. Of note, sample 1559B yields an εNd_{CHUR} value of +4, which is similar to values previously documented in Song et al. (2018) for recrystallized dolomite. Fig. 7c displays the initial Sr and Nd isotope compositions for pristine Bayan Obo dolomite samples investigated here and these are compared to reported Sr and Nd isotope results from other carbonatite complexes within China, and to the established fields for HIMU, EM I, DMM, and PREMA-like mantle components.

The Pb isotopic compositions for the Bayan Obo carbonates analyzed here are listed in Tables 5a and 5b and are compared to those for carbonates from Miaoya carbonatites in Fig. 8 (Çimen et al., 2018). Initial Pb isotope compositions yield narrow ranges for $^{206}Pb/^{204}Pb_{(i)}$ (15.85–16.46), $^{207}Pb/^{204}Pb_{(i)}$ (15.22–15.29), and $^{208}Pb/^{204}Pb_{(i)}$ (35.68–36.77), and overlap with those reported in Chen et al. (2020). These plot mostly in between the 1.2 and 1.4 Ga isochrons (Fig. 8a), a feature consistent with the accepted age of the H8 dolomite (1.3 Ga; Smith et al., 2015; Zhu et al., 2015; Chen et al., 2020).

4.4. Assessment of in-situ boron concentrations

Figs. 9 and 10 display the ^{11}B ion signal intensities (time-resolved plots) recorded for in-situ analyses of dolomite matrix and other phases (e.g., monazite, apatite) within Bayan Obo samples (1532 and 1649.5) by laser ablation (LA)-ICP-MS; similar results for samples 1551 and 1730 are listed in the supplementary information. These samples were selected for the detailed, in-situ investigations based on their petrographic/mineralogic nature and/or distinct boron isotopic compositions (Table 3). The location for each laser ablation spot analysis is identified on the associated μ-XRF map and corresponding ion signal intensities are listed in Supplementary Table 1. Laser ablation analyses conducted in raster mode are also presented as time resolved plots (Fig. 9c and 10b, c) as these were conducted over specific vein locations. The median, background subtracted ^{11}B ion signals for all single spot analyses along with their associated 2 sigma uncertainty are listed in Supplementary Table 1. The results indicate that the ^{11}B ion signals are relatively consistent and overlapping for both different phases (dolomite vs. REE-bearing monazite or apatite) and dolomite facies/matrices (CG vs. HG vs. FG). Median ^{11}B ion signal intensities for all dolomite spots range from 1136 to 2594 cps of ^{11}B, whereas median values for all REE-minerals range from 1907 to 2679 cps. Although these analyses are associated with large uncertainties, it is nonetheless clear that all spots analyzed yield ^{11}B ion signal intensities that are on the same order of magnitude. The sole exceptions are the secondary Ca-rich phase (spot #5) and oxide-rich area (spot #10) investigated in fine-grained sample 1730, which yielded higher ^{11}B ion signals; these two analyses are also associated with higher uncertainties due to their poor ablation characteristics (i.e., areas 'exploded' when hit with laser beam). As stated earlier, although not matrix matched, the calculated ion yields based on the ^{11}B ion signals for the different phases analyzed from the Bayan Obo samples (range from ~1700 to 3600 cps/ppm) are roughly similar to that calculated for the NIST SRM 610 external standard (~1300 cps/ppm).

Table 4
Strontium and neodymium isotope data on samples from Bayan Obo.

Sample	Type	Rb (ppm)	Sr (ppm)	$^{87}Rb/^{86}Sr$	$^{87}Sr/^{86}Sr$	2σ	$^{87}Sr/^{86}Sr$ *(i)*	Nd (ppm)	Sm (ppm)	$^{147}Sm/^{144}Nd$	$^{143}Nd/^{144}Nd$	2σ	$^{143}Nd/^{144}Nd$ *(i)*	εNd(*t*)
1508	FG	0.04	1100	0.00011	0.70424	0.00002	0.70424	257	18.3	0.0492	0.51136	0.00001	0.51094	0.6
1508B	FG	0.02	1252	0.00005	0.70411	0.00001	0.70411	418	36.4	0.0513	0.51135	0.00001	0.51091	-1.2
1559	FG	0.6	1552	0.00115	0.70311	0.00009	0.70309	500	111.1	0.1045	0.51146	0.00002	0.51057	-12.6
1559B	FG	2.2	629	0.01061	0.70460	0.00001	0.70441	246	16.6	0.0442	0.51151	0.00001	0.51113	4.0
1729	FG	0.7	1118	0.00194	0.70368	0.00003	0.70364	674	64.6	0.0577	0.51138	0.00001	0.51088	-1.5
1729B	FG	0.8	1012	0.00225	0.70308	0.00001	0.70304	367	31.5	0.0588	0.51146	0.00001	0.51096	1.2
1730	FG	0.7	432	0.00498	0.70309	0.00001	0.70300	282	23.0	0.0533	0.51141	0.00001	0.51095	0.6
1649.5	CG	0.04	1600	0.00007	0.70333	0.00001	0.70333	538	58.5	0.0739	0.51156	0.00001	0.51092	0.7
1666	CG	0.4	2754	0.00046	0.70327	0.00002	0.70326	141	29.6	0.1033	0.51142	0.00004	0.51053	-12.2
1666B	CG	0.02	1472	0.00004	0.70326	0.00001	0.70326	487	50.6	0.0620	0.51147	0.00001	0.51095	-0.4
1679	CG	0.1	1286	0.00023	0.70307	0.00002	0.70306	194	18.5	0.0787	0.51148	0.00002	0.51081	0.6
1679B	CG	0.1	1692	0.00018	0.70326	0.00001	0.70326	110	15.9	0.0876	0.51142	0.00001	0.51067	-5.4
1532	HG	0.3	1712	0.00055	0.70407	0.00001	0.70406	156	20.3	0.0749	0.51147	0.00001	0.51083	-3.0
1551	HG	1.9	1215	0.00468	0.70405	0.00004	0.70396	594	100.1	0.1166	0.51163	0.00001	0.51064	-3.7
1551B	HG	2.3	545	0.01251	0.70370	0.00001	0.70347	134	19.4	0.0875	0.51150	0.00001	0.51075	-4.0
1551.6	HG	0.7	1193	0.00187	0.70349	0.00001	0.70345	431	53.6	0.0741	0.51125	0.00002	0.51062	-6.8

$^{87}Rb/^{86}Sr$ and $^{147}Sm/^{144}Nd$ values were calculated based on ICP-MS-determined elemental abundances, which are associated with relative uncertainties of between 3 to 5% (2σ level). 1.3 Ga age was used for age correction calculations (see text for details).

Table 5a
Pb isotope data on samples from Bayan Obo.

Sample	Type	U (ppm)	Pb (ppm)	Th (ppm)	$^{206}Pb/^{204}Pb$	2σ	$^{207}Pb/^{204}Pb$	2σ	$^{208}Pb/^{204}Pb$	2σ
1508	FG	0.08	22.3	4.5	16.068	0.0008	15.248	0.0009	36.734	0.0026
1508B	FG	0.07	33.4	6.9	15.995	0.0005	15.234	0.0006	36.526	0.0018
1559	FG	0.38	114	2.6	15.972	0.0006	15.234	0.0007	36.303	0.0020
1559B	FG	0.05	41.6	6.5	15.969	0.0006	15.229	0.0007	36.774	0.0021
1729	FG	0.62	287	25.8	16.022	0.0007	15.242	0.0007	36.264	0.0019
1729B	FG	0.71	202	2.0	15.973	0.0005	15.232	0.0006	35.813	0.0019
1730	FG	0.06	78.3	2.4	15.976	0.0005	15.235	0.0007	36.799	0.0017
1649.5	CG	0.06	35.1	1.4	16.102	0.0006	15.247	0.0007	36.081	0.0019
1666	CG	0.04	27.9	1.1	16.139	0.0008	15.247	0.0010	36.387	0.0034
1666B	CG	0.02	101	0.6	16.149	0.0006	15.251	0.0007	36.184	0.0020
1679	CG	0.03	66.6	0.4	16.335	0.0004	15.277	0.0005	36.354	0.0014
1679B	CG	0.01	137	0.3	16.464	0.0004	15.291	0.0005	36.331	0.0014
1532	HG	0.24	12.9	2.7	16.100	0.0005	15.245	0.0005	37.210	0.0017
1551	HG	0.03	27.6	2.1	16.060	0.0005	15.249	0.0005	36.501	0.0013
1551B	HG	0.03	14.7	2.5	16.137	0.0008	15.251	0.0009	37.411	0.0023
1551.6	HG	0.14	34.7	11.3	16.041	0.0006	15.239	0.0006	38.135	0.0019

Table 5b
Pb isotope data on samples from Bayan Obo.

Sample	Type	$^{207}Pb/^{206}Pb$	2σ	$^{208}Pb/^{206}Pb$	2σ	$^{206}Pb/^{204}Pb$ (*i*)	$^{207}Pb/^{204}Pb$ (*i*)	$^{208}Pb/^{204}Pb$ (*i*)
1508	FG	0.94903	0.00001	2.286	0.00006	16.02	15.24	35.91
1508B	FG	0.95243	0.00002	2.284	0.00006	15.97	15.23	35.68
1559	FG	0.95377	0.00001	2.273	0.00005	15.93	15.23	36.21
1559B	FG	0.95367	0.00001	2.303	0.00005	15.95	15.23	36.13
1729	FG	0.95132	0.00002	2.263	0.00005	15.99	15.24	35.90
1729B	FG	0.95360	0.00001	2.242	0.00006	15.93	15.23	35.77
1730	FG	0.95362	0.00002	2.303	0.00005	15.97	15.23	36.67
1649.5	CG	0.94690	0.00002	2.241	0.00006	16.08	15.25	35.92
1666	CG	0.94471	0.00002	2.255	0.00010	16.12	15.25	36.22
1666B	CG	0.94443	0.00002	2.241	0.00006	16.15	15.25	36.16
1679	CG	0.93524	0.00001	2.225	0.00004	16.33	15.28	36.33
1679B	CG	0.92872	0.00001	2.207	0.00005	16.46	15.29	36.32
1532	HG	0.94691	0.00001	2.311	0.00005	15.85	15.22	36.36
1551	HG	0.94949	0.00001	2.273	0.00004	16.05	15.25	36.19
1551B	HG	0.94506	0.00002	2.318	0.00004	16.11	15.25	36.71
1551.6	HG	0.94998	0.00002	2.377	0.00006	15.99	15.23	36.77

5. Discussion

5.1. Igneous petrogenesis of H8 dolomite ore

Complicated by multiple geological processes, the interpretation of geochemical data in relation to Bayan Obo host dolomite's origin has sparked continuous debate about whether it represents a sedimentary or magmatic body (Smith et al., 2015; Fan et al., 2016; Yang et al., 2017). The two-stage petrogenetic model put forth by Fan et al. (2014), Smith et al. (2015), and Chen et al. (2020) for a Mesoproterozoic carbonatite intrusion followed by Caledonian-aged metasomatism leading to REE remobilization is further strengthened by the results of this study. Here, for the first time, the boron isotopic compositions of H8 carbonates reinforce the interpretation of a magmatic origin, especially

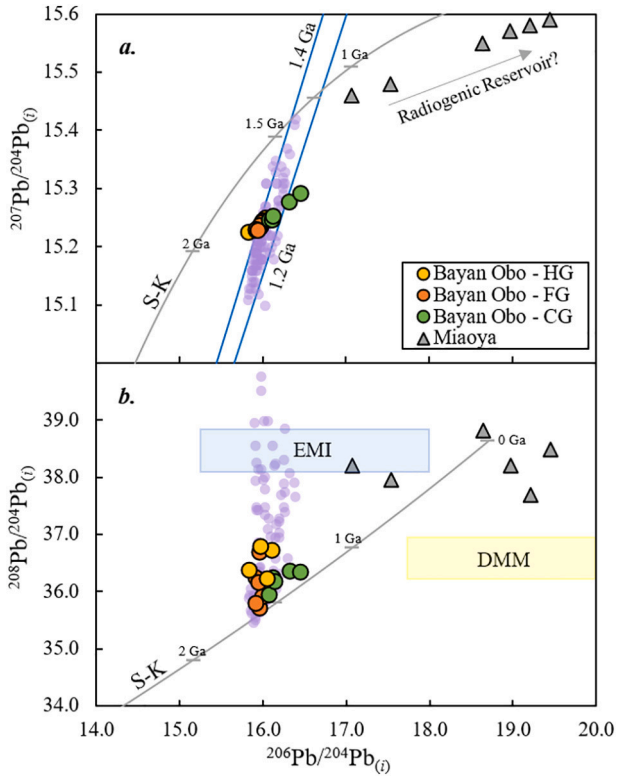

Fig. 8. (a) $^{207}Pb/^{204}Pb_{(i)}$ and (b) $^{208}Pb/^{204}Pb_{(i)}$ vs. $^{206}Pb/^{204}Pb_{(i)}$ values for Bayan Obo (this study) and Miaoya (Çimen et al., 2018) carbonates. Ages of 1.3 Ga for Bayan Obo (Smith et al., 2015) and 232 Ma for Miaoya (Çimen et al., 2018) have been adopted for initial Pb ratio calculations. Stacey and Kramers (1975) two-stage Pb evolution model (S–K) and initial Pb isotope ratios (purple circles) for in-situ analyses of Bayan Obo carbonates from Chen et al. (2020) are also plotted. EMI and DMM fields are from Zindler and Hart (1986). Associated analytical uncertainties are within the symbol size. (For interpretation of the references to colour in this figure legend, the reader is referred to the web version of this article.)

when combined with the results for traditional radiogenic (Sr, Nd, Pb) isotope systems.

The initial $^{87}Sr/^{86}Sr$ values range from 0.70300–0.70441 (Table 4) and are divided into two groups based on the petrographic designations reported in Chen et al. (2020); the first group, which is dominated primarily by samples exhibiting a coarse-grained (CG) dolomite matrix, are characterized by lower Sr isotope compositions (< 0.70340). These are deemed pristine or unaffected by later-stage hydrothermal alteration, and therefore indicative of derivation from an enriched mantle source compared to similarly-aged carbonatites worldwide (Fig. 11b; Bell and Simonetti, 2010). This is supported by the relatively high Sr concentrations of these dolomite samples (1012–2754 ppm; Table 4), which most likely buffered their inherited, mantle-derived Sr isotopic composition against possible crustal contamination or alteration as argued in previous carbonatite-related studies (e.g., Simonetti et al., 1998). Contrarily, the remaining dolomite samples analyzed here have generally lower Sr concentrations (545–1712 ppm) with correspondingly more radiogenic Sr isotopic ratios (0.70345–0.70441). The surrounding sedimentary carbonate rocks of Bayan Obo are characterized by much lower Sr abundances (129–165 ppm; Le Bas et al., 1997) and higher, more radiogenic Sr isotope compositions ($^{87}Sr/^{86}Sr$ = 0.71992–0.72620; Le Bas et al., 1997; Zhang et al., 2003). In Fig. 7a, the Sr concentrations of the dolomite samples studied here are plotted against their corresponding $\delta^{11}B$ values, and these define a negative trend that may represent mixing between CG (high Sr content) and FG samples (low Sr content). Thus, one possible explanation for this negative array is that it reflects Chen et al. (2020)'s proposed model where coarse-grained dolomite represents more 'pristine' carbonate and records the isotopic nature of their mantle source. In contrast, samples containing fine-grained and heterogeneous carbonate are likely to represent dolomite that was hydrothermally altered with radiogenic Sr being incorporated from surrounding sedimentary sources. This hydrothermal alteration may have, in turn, perturbed the boron isotopic signature of the dolomite samples. Hence, any evaluation of the mantle source characteristics for the Bayan Obo host dolomitic marble should be based solely on the samples containing 'pristine' dolomite, or those characterized by $^{87}Sr/^{86}Sr$ values < 0.70340 (as defined by Chen et al., 2020).

Based on their $^{87}Sr/^{86}Sr_{(i)}$ ratios (Table 4) reported here, samples 1559, 1649.5, 1666, 1666B, 1679, 1679B, and 1729B most likely represent pristine mineral assemblages, and these yield $\delta^{11}B$ values that

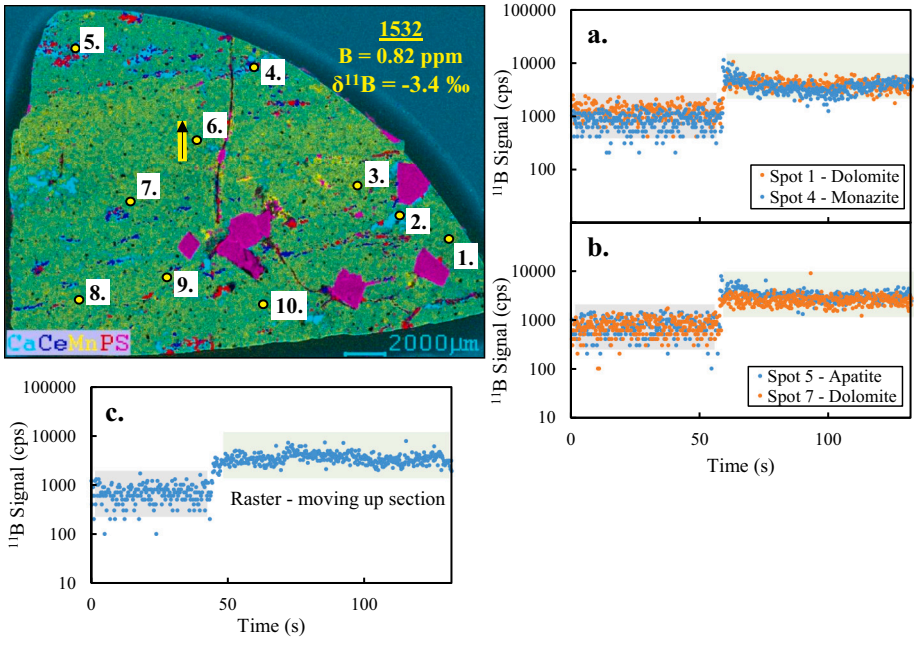

Fig. 9. Time-resolved laser ablation data for sample 1532 illustrating ^{11}B ion signal in various parts/phases of the thin section. µ-XRF map overlain with laser ablation spot locations (see supplementary information for all of the corresponding data). Arrow indicates direction of raster. (a-c) ^{11}B signal (cps) plotted vs. time of analysis (s). Fields indicate background (gray) and sample signal (green). (a-b) Signal comparisons between dolomite and REE minerals. (c) ^{11}B signal across raster. (For interpretation of the references to colour in this figure legend, the reader is referred to the web version of this article.)

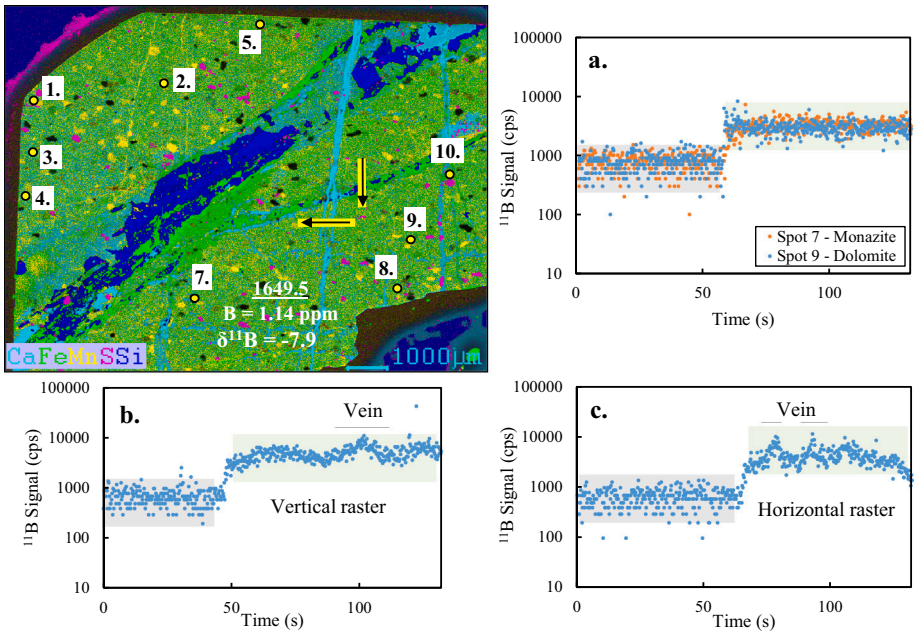

Fig. 10. Time-resolved laser ablation data for sample 1649.5 illustrating ^{11}B ion signal in various parts/phases of the thin section. μ-XRF map overlain with laser ablation spot locations (see supplementary information for all of the corresponding data). Arrow indicates direction of raster. (a-c) ^{11}B signal (cps) plotted vs. time of analysis (s). Fields indicate background (gray) and sample signal (green). (a) Signal comparisons between dolomite and REE minerals. (b-c) ^{11}B signal across raster. (For interpretation of the references to colour in this figure legend, the reader is referred to the web version of this article.)

range between −9.0 and −3.6‰ (Table 3); most of these samples belong to the CG group with the exception of 1559 and 1729B which have FG dolomite. A majority of these pristine dolomite samples are characterized by $\delta^{11}B$ values that overlap with those for asthenospheric mantle (−7.1 ± 0.9‰; Marschall et al., 2017; Fig. 7b), with the sole exception being sample 1666B, which yields a B isotope composition of −3.6‰. Thus, these $\delta^{11}B$ results support the hypothesis of Hulett et al. (2016) of limited incorporation of recycled crustal material within carbonatites older than 300 million years old (Fig. 11a).

Several samples analyzed here have conflicting isotopic signatures that diminish their usefulness for mantle source characterization. Specifically, sample 1730, has the lowest $^{87}Sr/^{86}Sr_{(i)}$ value (0.70300), but is also characterized by the lowest Sr content (432 ppm) and the heaviest $\delta^{11}B$ composition (+6.4‰). Moreover, the μ-XRF map for sample 1730 clearly displays several generations of carbonate (dolomite matrix + calcite vein) with the calcite vein containing higher B abundances (i.e., higher ^{11}B ion signals) than the surrounding dolomite (supplementary information Fig. S1 and Table S1); these features along with the lower Sr content all strongly suggest that its B isotope composition has been perturbed by secondary alteration. Thus, this result clearly demonstrates the ability of $\delta^{11}B$ compared to $^{87}Sr/^{86}Sr$ compositions in delineating the petrogenetic history of individual samples. In contrast, sample 1729 has the lightest $\delta^{11}B$ (−14.5‰) and highest TREE content (4016 ppm), which together suggest that this sample may have been subjected to an increased degree of REE ore-forming hydrothermal remobilization. This elevated concentration of TREEs compared to the highest reported from in-situ dolomite analyses (878 ppm; Chen et al., 2020) supports the notion of late-stage REE-minerals being included within the dolomite solution mode (whole rock) analyses, thus, potentially perturbing the isotope systems investigated here at the hand specimen scale. Moreover, the μ-XRF chemical map for sample 1729 (exhibited in supplementary information Fig. S2) illustrates the presence of significant Fe- and Ti-rich veins and secondary, Ca-rich areas that support its non-pristine nature. Furthermore, the data listed in Tables 3 and 4 indicate that the Sr, Nd, and B isotope ratios for most of the same depth interval pairs (e.g., 1551 and 1551B) do not replicate given their associated analytical uncertainties; thus, much care should be exerted with regard to interpreting the isotope results for dolomite samples from Bayan Obo in relation to delineating mantle source characteristics.

Stable isotopes signatures ($\delta^{13}C_{PDB}$, $\delta^{18}O_{SMOW}$) are also useful tracers in evaluating possible mantle source(s), contamination, or alteration from hydrothermal processes within carbonatite bodies (e.g., Deines, 1989; Keller and Hoefs, 1995). Based on the geological history of Bayan Obo, it is fitting to examine any possible perturbation of the stable isotope systems caused by late-stage REE enrichment processes (Fig. 5). There is no evident trend in the $\delta^{18}O_{SMOW}$ values vs. LREE concentrations for the Bayan Obo carbonates investigated here (Fig. 5a), whereas the carbonates from the Miaoya carbonatite complex (MCC) display a positive linear trend suggesting that the heavier $\delta^{18}O_{SMOW}$ values are attributed to the influence of late-stage REE-rich fluids (Çimen et al., 2018). In contrast, the $\delta^{11}B$ values for both carbonatite complexes do not exhibit positive trends with their respective LREE concentrations (Fig. 5b), which supports the overall interpretation that the $\delta^{11}B$ values for the vast majority of these carbonatites were not perturbed by late-stage REE mineralization. Admittedly, this does not rule out boron isotopic enrichment from hydrothermal processes as discussed above for altered Bayan Obo dolomite characterized by radiogenic strontium compositions (> 0.70340), and heavier boron isotopic compositions (up to −1.0‰). The documented isotopic variability within an individual depth (meter) interval of Bayan Obo's host dolomite (Chen et al., 2020) is also evident in the stable isotope compositions (Table 3). For example, the sample pair of 1729 and 1729B have $\delta^{13}C_{PDB}$ values that vary by ~1.0‰, whereas samples 1679 and 1679B have $\delta^{18}O_{SMOW}$ values that differ by 1.1‰. These differences are again consistent with Chen et al. (2020)'s argument that there is significant geochemical variability based on the degree of alteration experienced during the Caledonian-aged metasomatism.

Stable isotopes can also be used to evaluate any closed-system fractional crystallization process (e.g., Deines, 1989), which is one possible interpretation of the vertical array defined by the varying $\delta^{13}C_{PDB}$ and $\delta^{18}O_{SMOW}$ compositions with nearly constant asthenospheric $\delta^{11}B$ values for both Bayan Obo and MCC (Fig. 6b and c). However, as with the major and minor element data reported here (Fig. 3), the $\delta^{13}C_{PDB}$ vs. $\delta^{18}O_{SMOW}$ values from Bayan Obo do not plot along a unique Rayleigh fractional crystallization line (Fig. 6a). Çimen et al. (2018) also found no corroborating evidence for this closed system process based on data for carbonates from MCC. Therefore, it is possible that these C and O isotopic variations are inherited from the respective mantle source regions of both complexes. A comparison of the $\delta^{13}C_{PDB}$ and $\delta^{18}O_{SMOW}$ signatures for carbonates from Bayan Obo and MCC (Fig. 6a) reveals that those from Bayan Obo have heavier

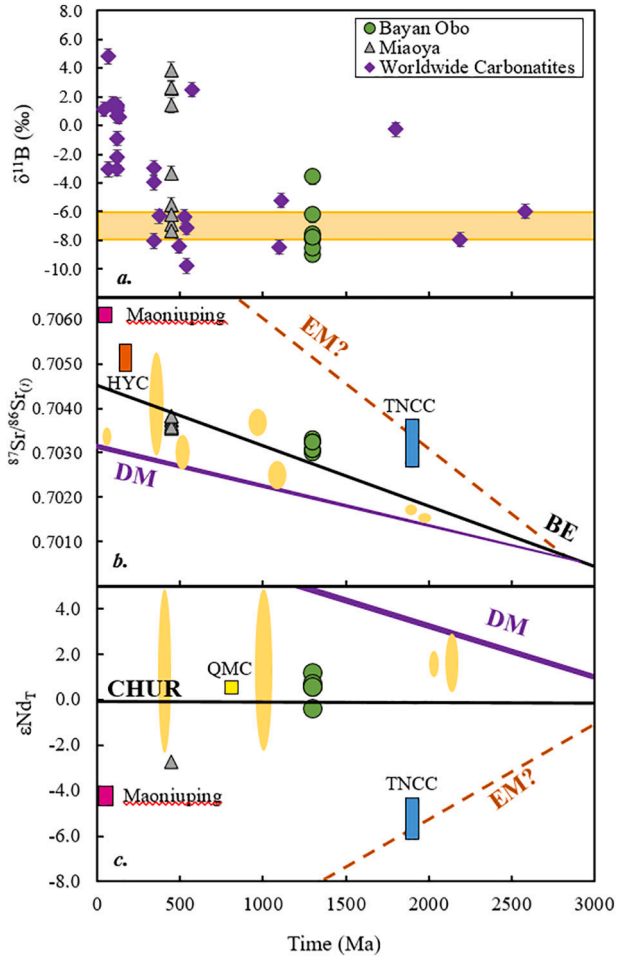

Fig. 11. (a) $\delta^{11}B$ (‰) values, (b) $^{87}Sr/^{86}Sr_{(i)}$ ratios, and (c) εNd_T values of 'pristine' Bayan Obo carbonates (this study) along with Miaoya carbonates (Çimen et al., 2018) are plotted vs. their respective emplacement ages in millions of years (Ma). (a) The $\delta^{11}B$ (‰) values for worldwide carbonatites are taken from Hulett et al. (2016) and Çimen et al. (2019). The shaded region represents the range in $\delta^{11}B$ compositions for MORB-like asthenospheric mantle (Marschall et al., 2017). (b) and (c) various rectangles indicates the range of initial strontium ratios or epsilon Nd values for Trans-North China Carbonatites (TNCC; blue; Xu et al., 2019), Maoniuping (pink; Xu et al., 2003), Huayangchuan (HYC; orange; Yu, 1992), and Qiganbulake mafic–ultramafic-carbonatite complex (QMC; yellow; Zhang et al., 2007). Bulk Earth (BE), Chondrite Uniform Reservoir (CHUR), Enriched Mantle (EM), and Depleted Mantle (DM) evolution lines are adapted from Bell and Simonetti (2010). Yellow fields in (b) and (c) indicate range in Sr and Nd isotope compositions, respectively, for various Canadian and Fennoscandinavian carbonatite complexes from Bell et al. (1982). Associated analytical uncertainties, where not visible, are within the symbol size. (For interpretation of the references to colour in this figure legend, the reader is referred to the web version of this article.)

signatures. This feature is consistent with the carbonates at Miaoya being mainly calcite (Su et al., 2019), whereas Bayan Obo's host body is dolomitic and hence preferentially incorporates the heavier ^{13}C and ^{18}O isotopes at magmatic temperatures (Deines, 1989). Of importance, this observation reveals that regardless of the dominant carbonate phase (calcite vs. dolomite) present within a mantle-derived carbonatite, pristine carbonate samples record asthenospheric mantle boron values. Admittedly, another possible factor in the reported heavier stable isotope signatures for the Bayan Obo carbonates is that the complex experienced more intense and pervasive metasomatism than Miaoya. This is evidenced in the multi-stage remobilization events that led to a greater degree of REE enrichment at Bayan Obo (up to ~3.65 wt% REE_2O_3) compared to Miaoya (Xu et al., 2010; Smith et al., 2015; Liu et al., 2018a, 2018b; Ren et al., 2019).

As stated earlier, the εNd_{CHUR} results can be divided into two categories, and these are 1- values for pristine samples that overlap with published data for the H8 dolomite (−1.5 to 1.2; Table 4 and Fig. 7c), and 2- values for carbonates (−3.0 to −12.6 and +4.0) that reflect the presence of micro-inclusions containing REE-bearing minerals within the dolomitic matrix. The inclusions are either older accessory minerals, younger monazites, or a combination of both. Previously published Sm–Nd data for common accessory minerals at Bayan Obo, such as aeschynite-(Ce), apatite, and aegerine, give 1.3 Ga age-corrected εNd_{CHUR} values ranging from −2.7 to −10.4 (Nakai et al., 1989; Philpotts et al., 1991; Wang et al., 1994). Based on the μ-XRF chemical maps obtained for the samples analyzed here, there are a significant number of accessory minerals present; REE-rich minerals (Ce), apatites (P), and Si-rich phases (Fig. 2). However, identifying the exact mineral (s) responsible for the radiogenic Nd isotopic signatures is further complicated by protracted monazite mineralization at Bayan Obo (Smith et al., 2015; Song et al., 2018). Song et al. (2018) proposed a model for the Nd isotopic evolution of the Bayan Obo host dolomite from a single source based on monazites that formed between 900 and 350 Ma. Using this model, the radiogenic εNd_{CHUR} results reported here overlap with those of monazites documented in Song et al. (2018), when recalculated for ages ranging from 900 to 450 Ma. Conversely, sample 1559B's εNd_{CHUR} value (+4.0), which does not overlap with monazite modelling, may represent a recrystallized dolomite (Song et al., 2018). In summary, the reported εNd_{CHUR} values from −3.0 to −12.6 could be attributed to the presence of either primary (1.3 Ga) or secondary (~450 Ma) non-carbonate minerals within the dolomite; therefore, Nd isotopic compositions for dolomite samples with εNd_{CHUR} = −1.5 to 1.2 could be used to evaluate the mantle source characteristics for Bayan Obo's host dolomite. However, these samples are further constrained when their corresponding initial $^{87}Sr/^{86}Sr$ ratios are considered resulting in a range of εNd_{CHUR} values (−0.4 to 1.2) for pristine dolomite that are indicative of derivation from a mixed mantle source (Figs. 7c and 11c). On the basis of the combined Nd and Sr isotope compositions for the samples of pristine dolomite (Fig. 7c), these may have been derived from a mixed upper mantle source consisting of HIMU- and EMI-like mantle components; a result that is consistent with the Nd and Sr isotope compositions for young (< 200 million years old) carbonatites worldwide (Bell and Simonetti, 2010).

Lastly, the bulk of the Pb isotope data for the carbonates analyzed here (Table 5a, b; Fig. 8) are tightly constrained and overlap well with the in-situ Pb isotope ratios reported in Chen et al. (2020). The Pb isotope system does not appear to have been greatly disturbed by Caledonian metasomatism as data plot within the 1.2 and 1.4 Ga isochrons reflecting a magmatic Mesoproterozoic age. However, Pb isotope data for sample 1532 plots slightly to the left of the isochrons, possibly representing minimal Pb loss during such a thermal event. Samples 1679 and 1679B plot slightly to the right of the isochrons perhaps due to the presence of accessory minerals (e.g., monazite, apatite) with higher contents of radiogenic Pb compared to the host dolomite (Fig. 8). Another possible explanation for the deviation of the $^{206}Pb/^{204}Pb_{(i)}$ values is that the dolomite samples are tapping a heterogeneous mantle source, which agrees with the vertical array shown in Fig. 8a. Variation in the $^{238}U/^{204}Pb$ ratio within the mantle source could be due to metasomatism, which has been documented in the geological history of the region (Smith et al., 2015; Chen et al., 2020). The vertical array in Fig. 8b showing variable $^{208}Pb/^{204}Pb_{(i)}$ with near constant $^{206}Pb/^{204}Pb_{(i)}$ is likely due to the preferential inclusion of Th over U in both the REE minerals and other U-Th-Pb bearing-minerals present at Bayan Obo (Zhu et al., 2015; Zhang et al., 2017; Zhang et al., 2019; Chen et al., 2020). This Th enrichment led to the accumulation of radiogenic ^{208}Pb within the carbonates since their Mesoproterozoic formation.

To evaluate the potential involvement of different reservoirs contributing to the variable isotopic signatures (Sr, Nd, Pb) reported for Bayan Obo's host dolomite, the Sr-Nd-Pb isotopic fields corresponding

to HIMU-, EMI-, DMM- (Depleted MORB Mantle) and PREMA-like (Prevalent Mantle) mantle fluid (Dixon et al., 2017) components are plotted in Figs. 7 (b, c) and 8b. HIMU and EMI mantle components (Zindler and Hart, 1986), which were derived based on the Sr-Nd-Pb isotope data from oceanic island basalts (OIBs), are often linked to the mantle source(s) and generation of younger (< 200 Ma) carbonatite melts (detailed summary in Bell and Simonetti, 2010). Based on the distribution of the B-Sr-Nd-Pb isotope data illustrated in Fig. 7 (b, c) and 8b, HIMU- and EMI-like mantle sources may also be involved in the derivation of Bayan Obo's host dolomite. Additionally, it is clear from Fig. 7 (b, c) and 8b that DMM is not a contributing mantle source component at Bayan Obo, but a PREMA-like mantle fluid component (Dixon et al., 2017) may be involved, in particular based on the distribution of the Sr and B isotope data (Fig. 7b). Alternatively, the heavier $\delta^{11}B$ values and more radiogenic Sr isotope ratios may be attributed to low degree partial melting of isotopically heterogeneous metasomatized and volatile-rich mantle since the latter is a prerequisite for carbonatite melt generation (e.g., Wallace and Green, 1988; Haggerty, 1989; Wyllie, 1989; Dalton and Wood, 1993). It has been advocated that the metasomatic activity associated with carbonatite magmatism may be linked to lithosphere-plume interaction (as discussed in Bell and Simonetti, 2010). Moreover, recent geochemical and isotopic (B and Mo) investigations of Cenozoic basaltic suites consisting of alkali basalts, nephelinites, and basanites from the North China Craton (NCC; Li et al., 2016, 2019) demonstrate the significance of metasomatic activity and/or fluid-fluxed melting in generating variable $\delta^{11}B$ values (range from ~-7.0 to ~-1.0‰) within their upper mantle source region. Of importance, on the basis of their combined trace element (e.g., Nb/B ratio) and isotopic compositions, the B isotopic variability cannot be attributed to the presence of a crustal component, or direct assimilation of continental crust during eruption (Li et al., 2016, 2019). Li et al. (2019) postulated that the origin of the carbonate-rich fluids within an intraplate setting of the NCC may be attributed to the decarbonization of subducted slabs stalled in the deep mantle. The degree of interaction between the slab-derived fluids from the deeper mantle, characterized by heavier $\delta^{11}B$ values (≥ −1‰), and overlying depleted upper mantle column (−7‰) determines the final B isotope composition and the degree of partial melting, which in turns controls the rock type generated (Li et al., 2019). As discussed in more detail later, Xu et al. (2018, 2019) postulate for the presence of an enriched mantle source resulting from large scale subduction and deep sediment recycling that was involved in the generation of the ~1800 million years old TNCC and associated alkaline silicate rocks; this was in response to the collision between the eastern and western sections of the NCC and related to the assembly of supercontinent Columbia.

Potential contamination from bulk continental crust or Bayan Obo Group sediments (i.e., limestone/shale; Rudnick, 1990; Marschall et al., 2017) is also evaluated in Fig. 7b. Given the combined Sr and B isotope characteristics for both crustal components (Fig. 7b), it is clear that the $^{87}Sr/^{86}Sr_{(i)}$ and $\delta^{11}B$ signatures for the Bayan Obo samples reported here cannot be readily attributed to their involvement (discussed in more detail below). In summary, the combined B-Sr-Pb isotope systematics for the Bayan Obo carbonates analyzed here are consistent with derivation of carbonatite magma from an isotopically heterogeneous mantle.

5.2. Micron-scale evaluation of the intra-sample boron distribution

In-situ LA-ICP-MS analyses (Figs. 9 and 10; Supplementary Table 1 and Supplementary Fig. 1) were performed to investigate the distribution of boron at high spatial resolution (100 s of micron scale) within four individual Bayan Obo samples of varied petrographic and isotopic nature in order to aid with the interpretation of the $\delta^{11}B$ results. Sample 1532 (Fig. 9) is a heterogeneous grained (HG) dolomite characterized by $\delta^{11}B$ value = −3.4‰ and $^{87}Sr/^{86}Sr_{(i)}$ = 0.70406, which categorizes it as an altered sample. The LA-ICP-MS results indicate no difference in the recorded ^{11}B ion signals between the main dolomite matrix compared to that for REE-bearing mineral phases (monazite and apatite; Fig. 9a, b). This confirms that there was no significant redistribution of B during the REE mineralization event. Additionally, the raster analysis conducted across several dolomite grains (Fig. 9c) shows a relatively smooth time-resolved laser ablation profile, and therefore suggests a homogeneous distribution of boron between dolomite grains. Thus, based on all of laser ablation analyses obtained for sample 1532 (Table S1), which indicate a relatively homogeneous distribution of boron, its $\delta^{11}B$ value of −3.4‰ cannot be attributed to simple Rayleigh fractional crystallization, or a similar magmatic/hydrothermal distillation process. In fact, from a boron abundance perspective, there is no evidence to suggest that sample 1532 is indeed altered (as per its Sr isotope composition), and therefore, the B and Sr isotope systematics may be decoupled. Sample 1649.5 is a 'pristine' coarse-grained (CG) dolomite characterized by an asthenospheric-like $\delta^{11}B$ value of −7.9‰ and $^{87}Sr/^{86}Sr_{(i)}$ = 0.70333. The time-resolved laser ablation data (Fig. 10) reveals similar findings to that for sample 1532; i.e., there are no significant differences in the ^{11}B ion signals recorded between both different phases (dolomite vs. monazite; Fig. 10a) or matrices (dolomite vs. Ca-Fe-rich vein; Fig. 10b, c). The two raster mode analyses from sample 1649.5 show small increases in ^{11}B ion signal when ablating across the Ca- or Fe/Ce-rich veins (Fig. 10c), but these are relatively minor and suggest only a minimal increase in B concentration. Hence, once again there is a lack of evidence in sample 1649.5 to suggest any type of boron elemental/isotopic fractionation due to Rayleigh or some sort of distillation process. In summary, the combined high spatial resolution time-resolved data reported here (Figs. 9, 10, and supplementary information) indicate that the $\delta^{11}B$ values (−9.0 to −3.6‰) for the pristine dolomite ($^{87}Sr/^{86}Sr$ < 0.7034) samples investigated here are inconsistent with fractionation associated with either the REE mineralization event or through some type of distillation process, but instead reflect mantle source isotopic heterogeneity; this may also be the case for HG sample 1532 ($\delta^{11}B$ = −3.4‰) despite its elevated Sr isotopic composition (0.70406).

Furthermore, to exhaust all possible explanations for the boron isotope values for 'pristine' samples that fall outside of the asthenospheric (MORB) mantle range (−7.1 ± 0.9‰; Marschall et al., 2017), two-component binary mixing calculations were conducted using various boron reservoirs/end members (Fig. 12). For example, one possible explanation for non-MORB-like boron signatures is crustal contamination, even though this interpretation was negated based on the radiogenic isotope results discussed earlier. Both average and upper continental crust reservoirs are boron enriched (10.5 and 43 ppm, respectively) relative to MORB (< 1 ppm), and are characterized by light $\delta^{11}B$ values (−10 and −8.8‰, respectively) based on global mass balance calculations (Marschall et al., 2017). As demonstrated in Fig. 12, it is difficult to reconcile the $\delta^{11}B$ values for the dolomite samples analyzed here with crustal contamination; in particular, since crust-MORB mixing lines fall within the asthenospheric mantle field (up to boron concentrations of ~1 ppm; Fig. 12). The modal percent of crustal involvement necessary to achieve the $\delta^{11}B$ values reported here ranges from 1 to 10%, which would have also resulted in correspondingly elevated (more radiogenic) Sr and Pb isotopic ratios that are not reported in this study. Additionally, the boron concentrations for the Bayan Obo carbonates are simply too low (0.4–1.14 ppm) to have been contaminated by continental crust, and are more consistent with MORB boron abundances within uncertainty (< 1 ppm; Chaussidon and Jambon, 1994; Marschall et al., 2017). Similarly, any contamination from S-type granites (sedimentary-source-type), which are characterized by $\delta^{11}B$ values that range from −20 to −8‰ and high B contents (up to 1 wt%; Trumbull and Slack, 2017), would result in both much higher abundances of B and radiogenic isotope signatures.

In contrast, seawater, carbonate sediments, and I-type (igneous source) granites have high boron concentrations (4.5, 13–26, and 5–7 ppm, respectively) and heavy $\delta^{11}B$ values (+39.6, +4.8 to +10.5,

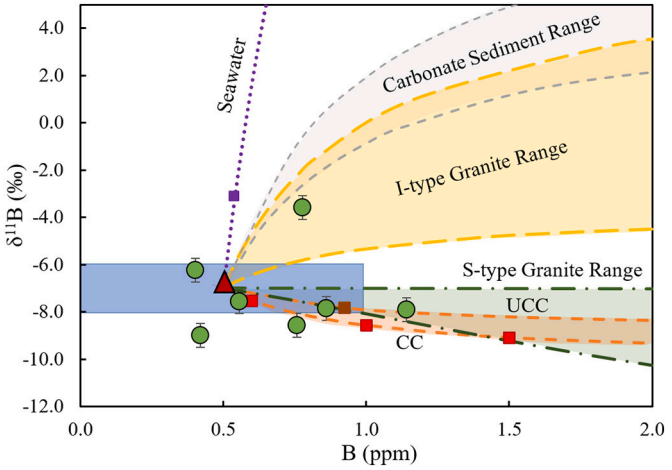

Fig. 12. Results of two component binary mixing calculations based on the $\delta^{11}B$ values and boron abundances for the 'pristine' dolomite samples analyzed here from Bayan Obo (green circles) and various terrestrial endmembers. For the calculations, asthenospheric (MORB) mantle was given an average B concentration of 0.5 ppm and $\delta^{11}B$ value = −7‰ (red triangle); the blue shaded region represents the range of values for 'fresh' MORBs as defined by Marschall et al. (2017). Squares along dashed lines represent 1, 5, and 10% mixing intervals between asthenospheric mantle and averaged upper and bulk continental crust and seawater end member components. B isotope compositions of continental crust (CC), upper continental crust (UCC), seawater, and carbonate sediments (gray field) are from Marschall et al. (2017), Foster et al. (2010), and Ishikawa and Nakamura (1993). Additional fields of I-type (yellow shaded region) and S-type (green shaded region) granite ranges are from Trumbull and Slack (2017). Mixing intervals are not shown for fields where B concentration data ranges. For example, a vast majority of the B isotope compositions reported for S-type granites were determined from tourmaline rather than whole rock analyses (Trumbull and Slack, 2017). (For interpretation of the references to colour in this figure legend, the reader is referred to the web version of this article.)

−4 to +6‰, respectively; Foster et al., 2010; Ishikawa and Nakamura, 1993; Trumbull and Slack, 2017), which may explain sample 1666B's heavier $\delta^{11}B$ value of −3.6‰ (Fig. 12). The two-component binary mixing results shown in Fig. 12 suggest that seawater was not involved in the petrogenesis of the Bayan Obo carbonates. This is an expected result as direct interaction with seawater is also not a plausible explanation from a regional tectonic perspective as the carbonatites at Bayan Obo are intrusive magmatic bodies and did not directly interact with seawater. Thus, a more likely scenario is that carbonate sediments enriched in ^{11}B, such as those plotted in the gray field, were either sampled by the carbonatite magma within its mantle source region or during emplacement as wall rock contamination from the surrounding Bayan Obo Group sediments. However, once again, sample 1666B does not have the elevated radiogenic Sr (0.70326; Table 4) and Pb isotopic ratios that would be expected with wall rock contamination. Overall, the various two-component binary mixing calculations conducted here cannot adequately explain the range of $\delta^{11}B$ values recorded for the Bayan Obo dolomite. Hence, this suggests that the variable $\delta^{11}B$ values reported here (−3.6 to −9.0‰; Table 3) for the 'pristine' dolomite samples analyzed most likely reflect boron isotope heterogeneity within their upper mantle source.

5.3. Temporal evolution of upper mantle, central China

The Bayan Obo and Miaoya carbonatite complexes (MCC) share similar emplacement and geological histories since both complexes involved initial carbonatite magmatism and emplacement that was followed (separated by hundreds of millions of years) by late-stage hydrothermal activity. However, they are distinct in age and REE-enrichment level with Bayan Obo reserves approximated at 40 Mt. (million tons) of 3–5.4 wt% REE_2O_3 (Smith et al., 2015), whereas Miaoya has estimated reserves of ~1.21 Mt. at an average grade of 1.72 wt% REE_2O_3 (Xu et al., 2010). Initial carbonatite intrusion at Bayan Obo occurred in the Mesoproterozoic (1.3 Ga; Smith et al., 2015), whereas Miaoya's emplacement is of Silurian age (at ~440 Ma; Ying et al., 2017; Zhang et al., 2019). This scenario therefore provides the opportunity to examine any possible temporal changes over a span of ~900 million years in the geochemical nature of the upper mantle source(s) that gave rise to carbonatite magmatism in central China. However, such a comparison assumes that their upper mantle sources share a common evolutionary history, which may not be the case given the complex tectonic processes that occurred in the region over a period of ~2 billion years and are outlined below.

Geographically, both complexes are located within central China, which consists of two major tectonic blocks, the North China Block and the South China Block, separated by the Qinling orogenic belt. Bayan Obo is located on the northern edge of the Northern China Block, whereas the MCC resides on the northern edge of the South China Block (Fig. 1 inset). This region experienced Mesoproterozoic rifting leading to the formation of the Bayan Obo host carbonatite and associated mafic dyke swarms (Yang et al., 2011 and references therein). Subsequent rifting during the Silurian opened the Mianlue Ocean and resulted in carbonatite generation (and associated mafic dyke swarms and syenite) at MCC, which coincides with the timing of the metasomatic activity at Bayan Obo (Ying et al., 2017; Su et al., 2019). The Permian-Triassic collision of the blocks, closed the ocean and formed one of the largest, ultra-high-pressure metamorphic zones (the Dabie-Sulu orogenic belt) aligning with the timing of the metasomatism that affected MCC (~240 Ma; Ying et al., 2017 and references therein).

Comparison of the B, C, and O isotope signatures for the carbonates from both MCC and Bayan Obo complexes outlined earlier offer similar observations/features, and these are; 1- neither complex shows evidence for dominant, closed-system melt differentiation, or significant crustal contamination, 2- there is evidence for B isotope heterogeneity in their respective mantle source(s), and 3- possible late-stage hydrothermal alteration produced enriched boron isotopic signatures for certain carbonate types. Çimen et al. (2018) alternatively suggested that the heavy $\delta^{11}B$ values (> +2‰) at MCC indicate the presence of recycled crustal material within its mantle source. This corroborates Hulett et al.'s (2016) hypothesis that young carbonatites (< 300 Ma) record heavier boron isotopic compositions due to the increased sampling of recycled crustal material within Earth's upper mantle with increasing geologic time. If one assumes that both Bayan Obo and MCC were derived from a similar upper mantle source region within central China, then the combined Sr isotope results from both complexes indicate that there is an enriched mantle component present beneath central China (Fig. 11b-c). Additionally, it may be argued that MCC experienced a greater influence of a PREMA-like mantle component/fluid than Bayan Obo, as many of the samples analyzed from MCC plot closer to the B–Sr isotope characteristics of this endmember (Fig. 7b).

The εNd_{CHUR} values for the carbonates from MCC (−1.1 to 0.1; Çimen et al., 2018) are similar to pristine dolomite samples from Bayan Obo (−0.4 to 1.2; excluding those with significant monazite or other mineral inclusions). However, Çimen et al. (2018) stated that late-stage hydrothermal alteration reset the Nd isotopic composition of MCC as the reported Sm–Nd errorchron yielded an age of ~151 Ma, which was attributed to the timing of a late-stage metasomatic event at MCC (232 ± 4.5 Ma; Ying et al., 2017). Therefore, Çimen et al. (2018) argued that there is only one sample analyzed from MCC that retained its original Nd composition (−2.7), which does not overlap with the initial Nd isotopic composition of the Bayan Obo carbonates believed to reflect the mantle source region (−0.4 to 1.2; Fig. 7c). Unfortunately, given the limited number of samples with reliable Nd isotope signatures from both Bayan Obo and Miaoya (Figs. 7c and 11c), it is difficult to delineate with a high degree of certainty any Nd isotopic temporal evolution in the upper mantle between ~1300 and ~440 million years

ago for central China.

Comparison of the initial Pb compositions for both complexes (Fig. 8) reveals that there was a significant change in the Pb composition (and corresponding $\mu = {}^{238}U/{}^{204}Pb$ value) of the upper mantle in this region over the ~900 million years between their respective periods of emplacement. Alternatively, it may simply suggest that their respective mantle sources are entirely distinct and do not share a common tectonic evolution. The initial Pb isotopic values for the Bayan Obo carbonates are notably more constrained than those from MCC (Fig. 8). The initial Pb compositions for the carbonates from MCC are extremely varied and require the input of a highly radiogenic end-member (e.g., $^{206}Pb/^{204}Pb_{(i)} = 17.07–41.21$). Çimen et al. (2019), Chen et al. (2018), and Andersen (1987) also document a similar type radiogenic component in the Pb isotope compositions for carbonatite complexes from Blue River (Canada), Shaxiongdong (China), and Fen (Norway), respectively, and postulated that it is of mantle origin. A plausible explanation for the generation of this distinct radiogenic Pb reservoir for Chinese carbonatite occurrences could be attributed to recent (post 1.3 Ga) metasomatism of subcontinental lithospheric mantle by Archean-to-early Proterozoic-aged subducted marine carbonates (Chen et al., 2018 and references therein). Moreover, the carbonate samples from Bayan Obo also depict a range in $^{206}Pb/^{204}Pb$ ratios$_{(i)}$ (Fig. 8a) that clearly suggest mantle source heterogeneity.

Fig. 11a displays the B isotope results obtained here for Bayan Obo carbonates in a global context since it compares the $\delta^{11}B$ values (and corresponding emplacement age) to those reported in Hulett et al. (2016) and Çimen et al. (2018, 2019). The $\delta^{11}B$ values for the 'pristine' carbonates from Bayan Obo, based on the $^{87}Sr/^{86}Sr_{(i)}$ values described above, are generally consistent with the model proposed in Hulett et al. (2016), which argues that carbonatites older than 300 Ma record typical asthenospheric mantle values ($-7.1 \pm 0.9‰$; Marschall et al., 2017). However, it is worth pointing out that sample 1666B records a heavier boron value ($-3.6‰$). Hulett et al. (2016) explains the positive "spikes" in heavier boron isotopic values at both ~1800 Ma and ~ 570 Ma as due to major orogenic/tectonic events involving supercontinent buildup and thus association with extensive periods of subduction, such as the suturing of Gondwana (~750 to 530 Ma) and the building of Columbia (~2 to 1.8 Ga). Similarly, break-up of the supercontinent Columbia under the NCC at ~1.3 Ga was accompanied by an increased rate of subduction of crustal material leading to greater boron isotopic heterogeneity in the upper mantle. Therefore, it is possible that the heavier boron signature of 1666B may be attributed to this latter event.

Further evidence for the presence of a heterogeneous mantle region beneath central China is documented in a recent study by Xu et al. (2019) that reported enriched initial Sr isotope ratios and εNd_{CHUR} values for Paleoproterozoic-aged Trans-North China Carbonatites (TNCC; Fig. 11b and c). Xu et al. (2018, 2019) argue that the TNCC and associated alkaline rocks sampled a mantle source enriched by deep sediment recycling brought on by the ~1810 Ma collision between the eastern and western sections of the NCC, which assembled the supercontinent Columbia. Thus, the isotopic results for carbonatites from the TNCC (Xu et al., 2019) and this study both indicate the presence of an enriched upper mantle beneath the NCC. The comparison of initial Sr isotope ratios for younger carbonatites, Maoniuping (26 Ma; Ling et al., 2016; Liu et al., 2019) and HYC (229 Ma; Xue et al., 2020) in Fig. 11b, supports the presence of recycled crustal material within the source region as the carbonatite complexes record enriched Sr isotopic signatures. This is also the case for the Nd isotopic compositions for the carbonatites at Maoniuping and QMC, even with the QMC's distal location in western China. Notably this contrasts with $^{87}Sr/^{86}Sr_{(i)}$ and εNd_{CHUR} results from other carbonatites (e.g., Canada; Bell et al., 1982) that are consistent with derivation from a depleted upper mantle source (Fig. 11b and c). Together these results suggest that large-scale subduction events associated with supercontinent formation/break-up led to the formation of a heterogeneous and enriched upper mantle source beneath the NCC prior to 2 billion years ago.

6. Conclusions

Here, the first-time reported $\delta^{11}B$ values for Bayan Obo's host dolomitic marble combined with radiogenic (Sr, Nd, Pb) and stable (C, O) isotope signatures support their igneous petrogenesis with carbonatite melts derived from a heterogeneous upper mantle source. The geochemical and isotopic data documented in this study are consistent with the petrogenetic model previously put forward for the derivation of H8 dolomite at Bayan Obo, which involved two major geological events. An initial carbonatite intrusion at ~1.3 Ga followed by a significant closed-system thermal event leading to the remobilization of REEs at ~400 Ma. The former involved rift-induced melting associated with the break-up of supercontinent Columbia, whereas the latter was caused by the opening of the Mianlue ocean during the Silurian. The initial mantle-derived carbonatite emplacement is recorded in the Sr, Pb, and B isotopic compositions, and the REE-remobilization event is revealed through Nd isotopic compositions and carbonate mineralogy.

The Pb isotope results reported here compared with those for carbonates from the younger Miaoya carbonatite complex indicate that the lead isotopic composition (and corresponding μ value) of the upper mantle beneath central China increased considerably over a period of ~900 million years (between ~1.3 and 0.4 Ga). This feature may be attributed to an increasing degree of metasomatism involving fluids/melts emanating from the underlying, convecting asthenosphere that contain both Sr-enriched phases (mantle carbonates) and U- and/or Pb-rich accessory minerals (e.g., Meen et al., 1989; Schmidberger et al., 2005) that impacted the overlying lithosphere. Alternatively, the Pb isotope compositions may simply indicate the presence of distinct lithospheric upper mantle sources that have coalesced together via plate tectonic processes during the past 2 billion years. Lastly, the combined (B, Sr, Pb) isotope data reported here for Bayan Obo pristine dolomite and those from previous studies for carbonatite complexes located within central China indicate the presence of enriched upper mantle sources that are at least 2 billion years old, and these most likely contain recycled crustal material.

Declaration of competing interest

The authors declare that they have no known competing financial interests or personal relationships that could have appeared to influence the work reported in this paper.

Acknowledgements

We thank Dr. Dana Biasatti (CEST) and Dr. Karl Cronberger for their assistance with C and O isotopes and EMP analyses, respectively. Dr. Troy Rasbury from Stony Brook University is thanked for providing the modern coral boron isotope standard. This research was financially supported by the University of Notre Dame. We also greatly appreciate the thoughtful comments provided by two anonymous reviewers and the editor, Dr. Catherine Chauvel.

Appendix A. Supplementary data

Supplementary data to this article can be found online at https://doi.org/10.1016/j.chemgeo.2020.119859.

References

Andersen, T., 1987. Mantle and crustal components in a carbonatite complex, and the evolution of carbonatite magma: REE and isotopic evidence from the Fen complex, S.E. Norway. Chem. Geol. Isotope Geosci. Sect. 65, 147–166.

Bai, G., Zhongxin, Y., 1985. Carbonatites and related mineral resources: Chinese Academy of Geological Sciences. Bull. Inst. Mineral Deposits 13, 107–140 [In Chinese, English

abstract, p. 189–192.].
Bailey, D.K., 1993. Carbonate magmas. J. Geol. Soc. Lond. 150, 637–651.
Balboni, E., Jones, N., Spano, T., Simonetti, A., Burns, P.C., 2016. Chemical and Sr isotopic characterization of North America uranium ores: Nuclear forensic applications. Appl. Geochem. 74, 24–32.
Bell, K., Blenkinsop, J., 1987. Archean depleted mantle-evidence from Nd and Sr initial isotope ratios of carbonatites. Geochim. Cosmochim. Acta 51, 291–298.
Bell, K., Simonetti, A., 1996. Carbonatite magmatism and plume activity: implications from the Nd, Pb and Sr isotope systematics of Oldoinyo Lengai. J. Petrol. 37, 1321–1339.
Bell, K., Simonetti, A., 2010. Source of parental melts to carbonatites–critical isotopic constraints. Miner. Petrol. 98, 77–89.
Bell, K., Tilton, G.R., 2001. Nd, Pb and Sr isotopic compositions of East African Carbonatites: evidence for mantle mixing and plume inhomogeneity. J. Petrol. 42, 1927–1945.
Bell, K., Blenkinsop, J., Cole, T.J.S., Menagh, D.P., 1982. Evidence from Sr isotopes for long-lived heterogeneities in the upper mantle. Nature 298, 251–253.
Bizzaro, M., Simonetti, A., Stevenson, R.K., David, J., 2002. Hf isotope evidence for a hidden mantle reservoir. Geology 30, 771–774.
Chao, E.C.T., Tatsumoto, M., Back, J.M., Minkin, J.A., McKee, E.H., Ren, Y., 1995. Multiple lines of evidence for establishing the mineral paragenetic sequence of the Bayan Obo rare earth ore deposit of Inner Mongolia, China. In: Maurice, Y.T. (Ed.), Proceedings of the International Association on the Geology of Ore Deposits. vol. 8. pp. 53–73.
Chaussidon, M., Jambon, A., 1994. Boron content and isotopic composition of oceanic basalts: geochemical and cosmochemical implications. Earth Planet. Sci. Lett. 259, 541–556.
Chen, W., Lu, J., Jiang, S.-Y., Ying, Y.C., Liu, Y.S., 2018. Radiogenic Pb reservoir contributes to the rare earth element (REE) enrichment in South Qinling carbonatites. Chem. Geol. 494, 80–95.
Chen, W., Liu, H.-Y., Lu, J., Jiang, S.-Y., Simonetti, A., Xu, C., Wen, Z., 2020. The formation history of the ore-bearing dolomite marble from the giant Bayan Obo Fe-REE-Nb deposit, Inner Mongolia: insights from micron-scale geochemical data. Mineral. Deposita 55, 131–146.
Çimen, O., Kuebler, C., Monaco, B., Simonetti, S.S., Corcoran, L., Chen, W., Simonetti, A., 2018. Boron, Carbon, Oxygen and Radiogenic Isotope Investigation of Carbonatite from the Miaoya complex, central China: evidences for late-stage REE hydrothermal event and mantle source heterogeneity. Lithos 322, 225–237.
Çimen, O., Kuebler, C., Simonetti, S.S., Corcoran, L., Mitchell, R., Simonetti, A., 2019. Combined boron, radiogenic (Nd, Pb, Sr), stable (C, O) isotopic and geochemical investigations of carbonatites from the Blue River Region, British Columbia (Canada): Implications for mantle sources and recycling of crustal carbon. Chem. Geol. 529. https://doi.org/10.1016/j.chemgeo.2019.07.015.
Cooper, A.F., Boztuğ, D., Palin, M.J., Martin, C.E., Numata, M., 2011. Petrology and petrogenesis of carbonatitic rocks in syenites from central Anatolia, Turkey. Contrib. Mineral. Petr. 161, 811–828.
Coplen, T.B., Kendall, C., Hopple, J., 1983. Comparison of stable isotope reference samples. Nature 302, 236–238.
Craig, H., 1957. Isotopic standards for carbon and oxygen and correction factors for mass-spectrometric analysis of carbon dioxide. Geochim. Cosmochim. Acta 12, 133–149. https://doi.org/10.1016/0016-7037(57)90024-8.
Dalton, J.A., Wood, B.J., 1993. The compositions of primary carbonate melts and their evolution through wallrock reaction in the mantle. Earth Planet Sci. Letter. 119, 511–525.
Deines, P., 1989. Stable isotope variations in carbonatites. In: Bell, K. (Ed.), Carbonatites: Genesis and Evolution. George Allen and Unwin, London, pp. 301–359.
Dixon, J.E., Bindeman, I.N., Kingsley, R.H., Simons, K.K., Le Roux, P.J., Hajewski, T.R., Swart, P., Langmuir, C.H., Ryan, J.G., Walowski, K.J., Wada, I., Wallace, P.J., 2017. Light stable isotopic compositions of enriched mantle sources: resolving the dehydration paradox. Geochem. Geophy. Geosy. 18, 3801–3839.
Fan, H.R., Hu, F.F., Yang, K.F., Pirajno, F., Liu, X., Wang, K.Y., 2014. Integrated U-Pb and Sm-Nd geochronology for a REE-rich carbonatite dyke at the giant Bayan Obo REE deposit, Northern China. Ore Geol. Rev. 63, 510–519.
Fan, H.R., Yang, K.F., Hu, F.F., Liu, S., Wang, K.Y., 2016. The giant Bayan Obo REE-Nb-Fe deposit, China: controversy and ore genesis. Geosci. Front. 7, 335–344.
Foster, G., Pogge von Strandmann, P.A.E., Rae, J.A.E., 2010. Boron and magnesium isotopic composition of seawater. Geochem. Geophys. Geosys. 11, Q08015.
Gaillou, E., Post, J.E., Rost, D., Butler, J.E., 2012. Boron in natural type IIb blue diamonds: chemical and spectroscopic measurements. Am. Mineral. 97, 1–18.
Gittins, J., Harmer, R.E., 2003. Myth and reality in the carbonatite–silicate rock association. Period. Mineral. 72, 19–26.
Haggerty, S.E., 1989. Mantle metasomes and the kinship between carbonatites and kimberlites. In: Carbonatites: Origin and Evolution, Bell K. George Allen and Unwin, London, pp. 546–560.
Hulett, S.R.W., Simonetti, A., Rasbury, E.T., Hemming, N.G., 2016. Recycling of subducted crustal components into carbonatite melts revealed by boron isotopes. Nat. Geosci. 9, 904–909.
Ishikawa, T., Nakamura, E., 1992. Boron isotope geochemistry of the oceanic crust from DSDP/ODP Hole 504B. Geochim. Cosmochim. Acta 56, 1633–1639.
Ishikawa, T., Nakamura, E., 1993. Boron isotope systematics of marine sediments. Earth Planet Sci. Letter. 117, 567–580.
Jenner, G.A., Longerich, H.P., Jackson, S.E., Fryer, B.J., 1990. ICP-MS—A powerful tool for high-precision trace-element analysis in Earth sciences: evidence from analysis of selected U.S.G.S. reference samples. Chem. Geol. 83, 133–148.
Jones, A.P., Genge, M., Carmody, L., 2013. Carbonate melts and carbonatites. Rev. Mineral. Geochem. 75, 289–322.
Kasemann, S., Erzinger, J., Franz, G., 2000. Boron recycling in the continental crust of the central Andes from the Paleozoic to Mesozoic, NW Argentina. Contrib. Mineral. Petrol. 140, 328–343.
Keller, J., Hoefs, J., 1995. Stable isotope characteristics of recent natrocarbonatites from Oldoinyo Lengai. Carbonatite Volcanism, IAVCEI Proceedings in Volcanology 4, 113–123.
Le Bas, M.J., Keller, J., Kejie, T., Wall, F.V., William, C.T., Peishan, Z., 1992. Carbonatite dykes at Bayan Obo, inner Mongolia, China. Miner. Petrol. 46, 195–228.
Le Bas, M.J., Spiro, B., Yang, X.M., 1997. Oxygen, carbon and strontium isotope study of the carbonatitic dolomite host of the Bayan Obo Fe-Nb-REE deposit, Inner Mongolia, N. China. Mineral. Mag. 61, 531–541.
Le Bas, M.J., Xueming, Y., Taylor, R.N., Spiro, B., Milton, J.A., Peishan, Z., 2007. New evidence from a calcite-dolomite carbonatite dyke for the magmatic origin of the massive Bayan Obo ore-bearing dolomite marble, Inner Mongolia, China. Miner. Petrol. 90, 223–248.
Lee, W.J., Wyllie, P.J., 1998. Processes of crustal carbonatite formation by liquid immiscibility and differentiation, elucidated by model systems. J. Petrol. 39, 2005–2013.
Lee, W.J., Fanelli, M.F., Cava, N., Wyllie, P.J., 2000. Calciocarbonatite and magnesiocarbonatite rocks and magmas represented in the system CaO-MgO-CO2-H2O at 0.2 GPa. Miner. Petrol. 68, 225–256.
Li, H.-Y., Zhou, Z., Ryan, J.G., Wei, G.-J., Xu, Y.-G., 2016. Boron isotopes reveal multiple metasomatic events in the mantle beneath the eastern North China Craton. Geochim. Cosmochim. Acta 194, 77–90.
Li, H.-Y., Li, J., Ryan, J.G., Li, X., Zhao, R.-P., Ma, L., Xu, Y.-G., 2019. Molybdenum and boron isotope evidence for fluid-fluxed melting of intraplate upper mantle beneath the eastern North China Craton. Earth Planet Sci. Letter. 520, 105–114.
Ling, X.X., Li, Q.L., Liu, Y., Yang, Y.H., Liu, Y., Tang, G.Q., Li, X.H., 2016. In situ SIMS Th-Pb dating of bastnaesite: constraint on the mineralization time of the Himalayan Mianning-Dechang rare earth element deposits. J. Anal. At. Spectrom. 31, 1680.
Liu, S., Fan, H.-R., Yang, K.-F., Hu, F.-F., Rusk, B., Liu, X., Li, X.-C., Yang, Z.-F., Wang, Q.-W., Wang, K.-Y., 2018a. Fenitization in the gialnt Bayan Obo REE-Nb-Fe deposit: Implication for REE mineralization. Ore Geo. Rev. 94, 290–309.
Liu, S., Fan, H.-R., Yang, K.-F., Hu, F.-F., Wang, K.-Y., Chen, F.-K., Yang, Y.-H., Yang, Z.-F., Wang, Q.-W., 2018b. Mesoproterozoic and Paleozoic hydrothermal metasomatism in the giant Bayan Obo REE-Nb-Fe deposit: constrains from trace elements and Sr-Nd isotope of fluorite and preliminary thermodynamic calculation. Precambrian Res. 311, 228–246.
Liu, Y., Chakhmouradian, A.R., Hou, Z., Song, W., Kynicky, J., 2019. Development of REE mineralization in the giant Maoniuping deposit (Sichuan, China): insights from mineralogy, fluid inclusions, and trace-element geochemistry. Mineral. Deposita 54, 701–718.
Marschall, H., Foster, G., 2017. Boron Isotopes: The Fifth Element. Adv. Iso. Geochem, Springer, Cham.
Marschall, H., Wanless, V.D., Shimizu, N., Pogge von Strandmann, P.A.E., Elliott, T., Monteleone, B.D., 2017. The boron and lithium isotopic composition of mid-ocean ridge basalts and the mantle. Geochim. Cosmochim. Acta 207, 102–138.
McCrea, J.M., 1950. On the isotopic chemistry of carbonates and a paleotemperature scale. J. Chem. Phys. 18, 849–857.
Meen, J.K., Ayers, J.C., Fregeau, E.J., 1989. Chapter 19: a model of mantle metasomatism by carbonated alkaline melts: trace-element and isotopic compositions of mantle source regions of carbonatitic and other magmas. In: Bell, K. (Ed.), Carbonatites: Genesis and Evolution. George Allen and Unwin, London, pp. 464–499.
Meng, Q.R., 1982. The genesis of the host rock dolomite of Bayan Obo iron ore deposits the analysis of its sedimentary environment. Geol. Rev. 28, 481–489 (in Chinese with English abstract).
Mitchell, R.H., 2005. Carbonatites and carbonatites and carbonatites. Can. Mineral. 43, 2049–2068.
Nakai, S., Masuda, A., Shimizu, H., 1989. La-Ba dating and Nd and Sr isotope studies on Bayan Obo rare earth element ore deposit, Inner Mongolia, China. Econ. Geol. 84, 2296–2299.
Philpotts, J., Tatsumoto, M., Li, X., Wang, K., 1991. Some Nd and Sr isotopic systematics for the REE-enriched deposit at Bayan Obo, China. Chem. Geo. 90, 177–188.
Ren, Y., Yang, X., Wang, S., Ozturk, H., 2019. Mineralogical and geochemical study of apatite and dolomite from the Bayan Obo giant Fe-REE-Nb deposit in Inner Mongolia: new evidences for genesis. Ore Geo. Rev. 109, 381–406.
Rudnick, R.L., 1990. Nd and Sr isotopic compositions of lower-crustal xenoliths from north Queensland, Australia: Implications for Nd model ages and crustal growth processes. Chem. Geo. 83 (3–4), 195–208. https://doi.org/10.1016/0009-2541(90)90280-K.
Schmidberger, S.S., Heaman, L.M., Simonetti, A., Creaser, R.A., Cookenboo, H.O., 2005. Formation of Paleoproterozoic eclogitic mantle, Slave Province (Canada): insights from in-situ Hf and U–Pb isotopic analyses of mantle zircons. Earth Planet Sci. Letter. 240, 621–633.
Simonetti, A., Goldstein, S.L., Schmidberger, S.S., Viladgar, S.G., 1998. Geochemical and Nd, Pb, and Sr isotope data from deccan alkaline complexes-inferences for mantle sources and plume–lithosphere interaction. J. Petrol. (11–12), 1847–1864.
Simonetti, A., Gariepy, C., Banic, C., Tanabe, R., Wong, H., 2004. Pb isotopic investigation of aircraft-sampled emissions from the Horne smelter (Rouyn, Quebec): implications for atmospheric pollution in northeastern North America. Geochim. Cosmochim. Acta 68, 3285–3294.
Smith, M.P., Campbell, L.S., Kynicky, J., 2015. A review of the genesis of the world class Bayan Obo Fe-REE-Nb deposits, Inner Mongolia, China: multistage processes and outstanding questions. Ore Geol. Rev. 64, 459–476.
Smith, E.M., Shirey, S.B., Richardson, S.H., Nestola, F., Bullock, E.S., Wang, J., Wang, W., 2018. Blue boron-bearing diamonds from Earth's lower mantle. Nature 560, 84–97.

Song, W.L., Xu, C., Smith, M.P., Chakmouradian, A.R., Brenna, M., Kynicky, J., Chen, W., Yang, Y.H., Deng, M., Tang, H.Y., 2018. Genesis of the world's largest rare earth element deposit, Bayan Obo, China: protracted mineralization evolution over ~1 b.y. Geology 46, 323–326.
Spivack, A.J., Edmond, J.M., 1987. Boron isotope exchange between seawater and the oceanic crust. Geochim. Cosmochim. Acta 51, 1033–1043.
Stacey, J.S., Kramers, J.D., 1975. Approximation of terrestrial lead isotope evolution by a two-stage model. Earth Planet. Sci. Lett. 26, 207–221.
Su, J.-H., Zhao, X.-F., Li, X.-C., Hu, W., Chen, M., Xiong, Y.-L., 2019. Geological and geochemical characteristics of the Miaoya syenite-carbonatite complex, Central China: implications for the origin of REE-Nb-enriched carbonatite. Ore Geo. Rev. 113, 103101.
Sun, S.-S., McDonough, W.F., 1989. Chemical and isotopic systematics of oceanic basalts: implications for mantle composition and processes. In: Saunders, A.D., Norry, M.J. (Eds.), Magmatism in Ocean Basins. Geol. Soc. London (Spec. Publ.), London.
Tanaka, T., Togashi, S., Kamioka, H., Amakawa, H., Kagami, H., Hamamotod, T., Yuhara, M., Orihashi, Y., Yoneda, S., Shimizu, H., Kunimaru, T., Takahashi, K., Yanagii, T., Nakano, T., Fujimaki, H., Shinjo, R., Asaharaa, Y., Tanimizu, M., Dragusan, C., 2000. JNdi-1: a neodymium isotopic reference in consistency with LaJolla neodymium. Chem. Geol. 168, 279–281.
Tao, K.J., Yang, Z.M., Zhang, P.S., Wang, W.Z., 1998. Systematic geological investigation on carbonatite dykes in Bayan Obo, Inner Mongolia, China. Sci. Geol. Sin. 33, 73–82 (in Chinese with English abstract).
Trumbull, R.B., Slack, J.F., 2017. Boron isotopes in the continental crust: granites, pegmatites, felsic volcanic rocks, and related ore deposts. In: Boron Isotopes: The Fifth Element. Adv. Iso. Geochem. Springer, Cham, pp. 249–272.
Tu, G.Z., Zhao, Z.H., Qiu, Y.Z., 1985. Evolution of Precambrian REE mineralization. Precambrian Res. 27, 131–151.
Veksler, I.V., Petibon, C., Jenner, G.A., Dorfman, A.M., Dingwell, D.B., 1998. Trace element partitioning in immiscible silicate–carbonate liquid systems: an initial experimental study using a centrifuge autoclave. J. Petrol. 39, 2095–2104.
Wallace, M.E., Green, D.H., 1988. An experimental determination of primary carbonatite magma composition. Nature 335, 343–346.
Wang, J.W., Tatsumoto, M., Li, X.B., Premo, W.R., Chao, E.C.T., 1994. A precise Th-232-Pb-208 chronology of fine-grained monazite-age of the Bayan Obo REE-FE-NB ore deposit, China. Geochim. Cosmochim. Acta 58, 3155–3169.
Woolley, A.R., 1989. The spatial and temporal distribution of carbonatites. In: Bell, K. (Ed.), Carbonatites: Origin and Evolution. George Allen and Unwin, London, pp. 15–37.
Woolley, A.R., Kjarsgaard, B.A., 2008. Carbonatite Occurrences of the World: Map and Database. Geological Survey of Canada. Open File Report 5796.
Wyllie, P.J., 1989. Origin of carbonatites: Evidence from phase equilibrium studies. In: Bell, K. (Ed.), Carbonatites: Origin and Evolution. George Allen and Unwin, pp. 500–545.
Xu, C., Huang, Z., Liu, C., Qi, L., Li, W., Guan, T., 2003. Geochemistry of carbonatites in Maoniuping REE deposit, Sichuan province, China. Sci. China Ser. D-Earth Sci. 46, 246–256.
Xu, C., Kynicky, J., Chakmouradian, A.R., Campbell, I.H., Allen, C.M., 2010. Trace element modeling of the magmatic evolution of rare earth-rich carbonatite from the Miaoya deposit, Central China. Lithos 118, 145–155.
Xu, C., Kynicky, J., Song, W., Tao, R., Lu, Z., Li, Y., Yang, Y., Pohanka, M., Galiova, M.V., Zhang, L., Fei, Y., 2018. Cold deep subduction recorded by remnants of a Paleoproterozoic carbonated slab. Nature Comm. 9 (2790), 1–8.
Xu, C., Chakmouradian, A.R., Kynicky, J., Li, Y., Song, W., Chen, W., 2019. A Paleoproterozoic mantle source modified by subducted sediments under the North China craton. Geochim. Cosmochim. Acta 245, 222–239.
Xue, S., Ling, M.-X., Liu, Y.-L., Kang, Q.-Q., Huang, R.-F., Zhang, Z.-K., Sun, W., 2020. The formation of the giant Huayangchuan U-Nb deposit associated with carbonatite in the Qinling Orogenic Belt. Ore Geol. Rev. 122, 103498.
Yang, X.M., Le Bas, M.J., 2004. Chemical compositions of carbonate minerals from Bayan Obo, Inner Mongolia, China: implications for petrogenesis. Lithos 72, 97–116.
Yang, X.Y., Sun, W.D., Zhang, X.Y., Zheng, Y.F., 2009. Geochemical constraints on the genesis of the Bayan Obo Fe-Nb-REE deposit, Inner 727 Mongolia, China. Geochim. Cosmochim. Acta 73, 1417–1435.
Yang, K.F., Fan, H.R., Santosh, M., Hu, F.F., Wang, K.Y., 2011. Mesoproterozoic carbonatitic magmatism in the Bayan Obo deposit, Inner Mongolia, North China: constraints for the mechanism of super accumulation of rare earth elements. Ore Geol. Rev. 40, 122–131.
Yang, X.Y., Lai, X.D., Pirajno, F., Liu, Y.L., Ling, M.X., Sun, W.D., 2017. Genesis of the Bayan Obo Fe-REE-Nb formation in Inner Mongolia, North China Craton: a perspective review. Precambrian Res. 288, 39–71.
Yang, K., Fan, H., Pirajno, F., Li, X., 2019. The Bayan Obo (China) giant REE accumulation conundrum aelucidated by intense magmatic differentiation of carbonatite. Geology 47.
Ying, Y., Chen, W., Lu, J., Jiang, S.Y., Yang, Y., 2017. In situ U–Th–Pb ages of the Miaoya carbonatite complex in the South Qinling orogenic belt, central China. Lithos 290-291, 159–171.
Yu, X., 1992. Geological, petrol-mineralogical characteristics and origin of the carbonatites from Huayangchuan, Shaanxi Province. Earth Sci.-J. China Uni. Geosci. 17, 151–158 (in Chinese with English abstract).
Yuan, Z.X., Bai, G., Wu, C.Y., Zhang, Z.Q., Ye, X.J., 1992. Geological features and genesis of the Bayan Obo REE Ore Deposit, Inner-Mongolia, China. Appl. Geochem. 7, 429–442.
Zhai, M.G., 2004. 2.1e1.7 Ga geological event group and its geotectonic significance. Acta Petrol. Sin. 20, 1343–1354 (in Chinese with English abstract).
Zhang, P., Yang, Z., Tao, K., Yang, X., 1996. Mineralogy and Geology of Rare Earths in *China*. Science Press, Beijing, pp. 226.
Zhang, Z.Q., Yuan, Z.X., Tang, S.H., Bai, G., Wang, J.H., 2003. Age and Geochemistry of the Bayan Obo Ore Deposit. Geological Publishing House, Beijing, pp. 222 (in Chinese with English abstract).
Zhang, C.-L., Li, X.-H., Li, Z.-X., Lu, S.-N., Ye, H.-M., Li, H.-M., 2007. Neoproterozoic ultramafic–mafic-carbonatite complex and granitoids in Quruqtagh of northeastern Tarim Block, western China: geochronology, geochemistry and tectonic implications. Precambrian Res. 152, 149–169.
Zhang, S.H., Zhao, Y., Li, Q.L., Hu, Z.C., Chen, Z.Y., 2017. First identification of baddeleyite related/linked to contact metamorphism from carbonatites in the world's largest REE deposit, Bayan Obo in North China Craton. Lithos 284-285, 654–665.
Zhang, W., Chen, W.T., Gao, J.-F., Chen, H.-K., Li, J.-H., 2019. Two episodes of REE mineralization in the Qinling Orogenic Belt, Central China: in-situ U-Th-Pb dating of bastnäsite and monazite. Mineral. Deposita 1–18.
Zhao, G.C., Sun, M., Wilde, S.A., Li, S.Z., 2003. Assembly, accretion and breakup of the Paleo-Mesoproterozoic Columbia Supercontinent: records in the North China Craton. Gondwana Res. 6, 417–434.
Zhu, X.K., Sun, J., Pan, C.X., 2015. Sm-Nd isotopic constraints on rare-earth mineralization in the Bayan Obo ore deposit, Inner Mongolia, China. Ore Geol. Rev. 64, 543–553.
Zindler, A., Hart, S.R., 1986. Chemical dynamics. Annu. Rev. Earth Pl. Sc. 14, 493–571.